

CAD of Solid Carbide End-Mills and its Applications

Chun Du

A Thesis

in

the Department

of

Mechanical & Industrial Engineering

Presented in Partial Fulfillment of the Requirements

for the Degree of Master of Applied Science (Mechanical Engineering) at

Concordia University

Montreal, Quebec, Canada

April 2011

© CHUN DU, 2011

CONCORDIA UNIVERSITY
School of Graduate Studies

This is to certify that the thesis prepared

By: Chun Du

Entitled: CAD of Solid Carbide End-Mills and its Applications

and submitted in partial fulfillment of the requirements for the degree of

Master of Applied Science

complies with the regulations of the University and meets the accepted standards with respect to originality and quality.

Signed by the final examining committee:

_____ Dr. C.Y Su _____ Chair

_____ Dr. H.D NG _____ Examiner

_____ Dr. W. Tian _____ Examiner

_____ Dr. C.Z. Chen _____ Supervisor

Approved by _____ Dr. A.K.W. Ahmed _____
Chair of Department or Graduate Program Director

_____ Dean Robin Drew _____
Dean of Faculty

Date _____ 13th, May, 2011 _____

Abstract

CAD of Solid Carbide End-Mills and its Applications

Chun Du

Nowadays, carbide end mills are widely utilized in the aluminum, titanium and steel cutting industries, so the more and more high-precision requirements to design of cutters are provided by users. Meanwhile, in order to finish the simulation and analysis of cutting processing, it is also important to design more free-control geometry model, and then transit into the CAD/CAM systems. For this purpose, many research works have been successfully conducted on optimizing the geometry model of cutters to get more real and easy controlled geometry; however, another critical factor, there are still more space to optimize the geometry model of cutters. To finish this task, in this work, first, a method has been established and implemented in the MATLAB to convert mathematic model into a free-form geometry model. Then, an accurate calculation system of area moment inertial of cutter is built. Finally, a detailed discussion on the cutting force of end-mills is provided, based on cutting simulation software. The major contributions of this work include the free-form end-mill modeling, which can render the 3-D geometric model of an end-mill in CATIA system, and a type of calculation of cutter area moment of inertial. This work can be used, together with an existing cutting force calculation method, to accurately predict cutting force during milling in order to get better geometry model of cutter. Meanwhile, solid modelling of the helical cutting tool can be carried out with computer graphics programming. It can also provide more precise 3-D solid models of end-mills for machining simulation by using finite element software.

Acknowledgements

I would like to say thanks to my supervisor, Dr. Zezhong C. Chen, for his guidance and support for this research topic. I really appreciate his enthusiasm, encouragement, expertise, and research philosophy. To Shuangxi Xie, Maqsood, and Jiang Zhu, I give my thanks for their encouragement, their valuable insight, and their comments.

Contents

Chapter 1	Introduction	1
1.1	Solid carbide end-mills	1
1.2	B-spline Curves	2
1.2.1	B-Spline Background.....	2
1.2.2	Application and Capabilities	4
1.2.3	Advantages	5
1.3	Parametric Design	6
1.3.1	Definition	6
1.3.2	Parametric Part Design and Modeling	7
1.4	Area Moment of Inertia.....	8
1.5	Literature Review	9
1.6	Objectives of the Thesis.....	12
1.7	Outline of the Thesis.....	12
Chapter 2	Parametric Modeling of the Side Cutting Edge of the Flute	14
2.1	List of Nomenclature of the Parametric Model	14
2.2	Parametric Representation of the Cutting Surfaces	15
2.2.1	Radius of the Toroidal Cutting Surface.....	16
2.2.2	Radius of the Conic Cutting Surface	16

2.2.3	Parametric Equation of Cutting Surface	17
2.3	Differential Form of the Cutting Edge	17
2.3.1	Helical Cutting Edge of the Toroidal Cutting Surface	19
2.3.2	Helical Cutting Edge of the Conic Cutting Surface	22
2.4	Explicit Equation of the Lag Angle of the Cutting Edge.....	25
2.4.1	Lag Angle of the Cutting Edge of the Toroidal Cutting Surface.....	25
2.4.2	Lag Angle of the Cutting Edge of the Conic Cutting Surface	27
2.5	Cutting Edge Representation with a B-Spline	29
2.5.1	Cutting Edge Representation with a Taylor's Series	29
2.5.2	Conversion of Taylor's Series to B-Splines	31
2.6	Application and Analysis.....	32
Chapter 3	Parametric Modeling of the Solid Cutter Flutes	37
3.1	List of Nomenclature of the Parametric Model	37
3.2	Introduction.....	37
3.3	The Coordinates of the Intersection Points of Cutting Flute	39
3.4	The 3D Models of Cutting Tools	44
Chapter 4	Area Moments of Inertia of Carbide Cutters	45
4.1	List of Notation and Introduction	45
4.2	Representation of Splines.....	46
4.3	Differential Method.....	48

4.3.1	Portion A	48
4.3.2	Portion B	50
4.4	Calculation of Area Moment of Inertia	51
4.5	Calculate of Area Moment of Inertia on the Gash and the Neck	56
4.6	Result Analysis	62
4.6.1	Influence of the Cutting Flutes	62
4.6.2	Influence of the Cutting Radius	65
4.6.3	The Results on the Gash and the Neck.....	68
4.6.4	Comparision between Two Different Methods	69
Chapter 5	Applications	71
5.1	Introduction	71
5.2	Influence of the Rake Angle to Area Moment of Inertia.....	72
5.3	Cutting Force Analysis based on the Change of Rake Angle	73
5.4	Cutting Force Analysis based on the Change of Helical Angles.....	75
Chapter 6	Conclusions and Future Research	78
6.1	Conclusions.....	78
6.2	Future Research.....	79
Chapter 7	References	80

List of Tables

Table 2.1 The parameter values of a solid carbide fillet tapered end-mill	33
Table 2.2. Results analysis of conversion of the analytical equation into B-splines	34
Table 2.3. Comparison between new conversion method and conventional method.....	36
Table 4.1. Area of moment of inertia of different end-mills.....	63
Table 4.2. Data for symmetric section fillet tapered end mills	66
Table 4.3. The area moment of inertia on the gash and on the neck	68
Table 4.4. The calculation efficiency	70
Table 5.1. Comparison of the effect of the rake angle.....	72
Table 5.2. The parameters of cutter and the geometry of workpiece	74
Table 5.3. The parameters of simulation.....	74
Table 5.4. The parameters of cutter and the geometry of workpiece.....	76

1.1 Solid carbide end-mills

An end-mill is a type of milling cutter, a cutting tool used in industrial milling applications. An end-mill can generally cut in all directions, except axially direction. End-mills are used in milling applications such as profile milling, tracer milling, face milling, and plunging. Meanwhile, tungsten carbide (WC) is an inorganic chemical compound containing equal parts of tungsten and carbon atoms. Generally, tungsten carbide is often simply called carbide. Tungsten carbide is approximately three times stiffer than steel, and is much denser than steel or titanium. Carbide cutting surfaces are often used for machining through materials such as carbon steel or stainless steel, as well as in situations where other tools would wear away, such as high-quantity production runs. Carbide generally produces a better finish on the part, and allows faster machining. Carbide tools can also withstand higher temperatures than standard high speed steel tools. The material is usually called cemented carbide, hard metal or tungsten-carbide cobalt: it is a metal matrix composite where tungsten carbide particles are the aggregate and metallic cobalt serves as the matrix. Therefore, solid carbide end-mills are a kind of end-mills with carbide material. Usually we use high speed steel to make tools but for some materials that are not easily cut, tungsten carbide comes. This kind of tools is suitable for cast iron, cast steel, carbon steel, alloy steel, quenched steel in CNC machining.

1.2 B-spline Curves

To model free-form shapes with a parametric representation in computer-aided design (CAD), B-spline curves are often used, and they are a major function in commercial CAD/CAM software. B-spline curves mathematically are parametric piecewise polynomials, thus, a B-spline curve can well represent complex shapes by specifying a number of control points. It is also very easy to modify the curve shape by changing the locations of the control points. In the conventional methods, a complex shape is usually represented with a large number of points, which make it difficult to manipulate and process the shape. Now, the commercial CAD/CAM software systems have the B-spline curve function; therefore, complex geometries can be represented more accurately, and they can be processed more easily, such as Boolean operations and meshing for finite element analysis. Since, in this research, B-spline curves are employed to represent the complex flute geometry of cutting tools, B-spline curves are introduced in detail in this section.

1.2.1 B-Spline Background

B-spline curves are a special type of spline curve, which was originally developed for ship building. In order to plot a smooth curve through a set of points, ship hull designers found a way through these points. They placed some metal weights called ducks at these points, and bent a thin metal or wooden beam called a spline through these weights. A spline is illustrated in Fig 1.1. It is evident that each weight affects the spline shape at the contacting

point the most and has less effect on the spline shape that is away from it. Based on the concept, the spline theory was established.

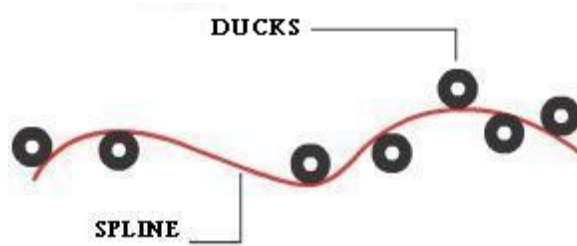


Figure 1.1. Illustration of a craftsman's wooden spline.

Among the published papers, in 1946, Schoenberg [1] first established the spline mathematical model with smooth piecewise polynomials and found that the cubic polynomial spline is an accurate mathematical representation of the draftsman's wooden beam. In the 1960s, Bézier proposed a free-form curve representation, Bezier curves. Then, the polynomials were extended to basis splines (B-splines). Eventually, non-uniform rational basis splines (NURBS) were proposed to represent the analytical curves, such as circles, ellipses, and parabolas, etc., and free-form curves, such as ship hulls, impellor blades, and automotive bodies, etc. Bezier and B-spline curves are special cases of the NURBS curves. At beginning, NURBS curves were only used in the proprietary CAD packages of the automotive companies. Gradually, NURBS curves became a mathematical model commonly used in commercial CAD/CAM software for generating and representing curves and surfaces. It is very important to represent complex shapes in mechanical design and modeling.

1.2.2 Application and Capabilities

Thanks to the unique features of NURBS curves, they are widely applied to the following areas:

- 1) Computer-aided design and manufacture,
- 2) Computer vision and robotics,
- 3) Imaging and visualization,
- 4) Biosciences, chemistry, physics, geophysics, and meteorology,
- 5) Bio-medical engineering, and
- 6) Business and social sciences

NURBS curves are mainly used for the following functions:

- 1) Parametric modeling of complex curves and surfaces,
- 2) Interpolation,
- 3) Approximation of functions,
- 4) Smoothing noisy data,
- 5) Solution of PDE's, and
- 6) Compression and denoising for the image process.

For interpolation, spline curves are often preferred because they can yield accurate results even using low degree polynomials without Runge's phenomenon. In curve fitting, NURBS

curves are used to approximate complex shapes. NURBS curves are a popular model in computer graphics.

1.2.3 Advantages

Compared to the analytical curves, the NURBS curves have the following advantages:

- 1) Easy to enumerate points on curve or surface,
- 2) Possible to describe complex shapes,
- 3) Easy to compute,
- 4) Infinitely differentiable,
- 5) Flexibility, and
- 6) Easy to control

However, the NURBS curves have the following disadvantages:

- 1) Control mesh must be quadrilaterals,
- 2) Continuity constraints difficult to maintain, and
- 3) Hard to find NRUBS curve intersections.

1.3 Parametric Design

1.3.1 Definition

Usually, a mechanical part consists of several geometric features related to its function and its manufacturing method. Now, a kernel technique of the computer-aided design is parametric part design and modelling. In light of a new trend of mechanical part design – the part feature optimization, feature-based parametric part design is a dispensable advanced technique since the parametric CAD models of the part features can be easily modified in the part design optimization process. Thus, the parametric part modelling function in the commercial CAD/CAM software is quite important. By definition, the parametric part design is to determine the key feature dimensions as the parameters and to specify the relationships (or constraints) among the parameters and other part dimensions. In the parametric modelling function of the CAD/CAM software, the functions of defining parameters and constraints are developed, and the parametric part models can be constructed without much effort. By assigning data to the feature parameters, all part

dimensions are calculated, and the solid model of the part can be changed accordingly and updated in seconds.

1.3.2 Parametric Part Design and Modeling

Mechanical part design includes a number of decision-making processes and activities, which are involved in determining the shape and dimensions of a mechanical part. Generally, the development of a mechanical part has five phases: formulation, concept design, configuration design, parametric design, and detail design. The parametric design is now crucial. With a parametric design of a part, the solid model of a part design can be easily attained, and the part can be analyzed in a virtual working environment to understand or predict the part performance and functionality. This can greatly reduce the leading time in the part design cycle and the cost of making prototype. To implement the parametric part design and modeling, the following five steps are necessary, which are

- 1) to define the key dimensions as the parameters,
- 2) to define the relationships or constraints between the parameters and the part dimensions,
- 3) to establish the part model with CAD/CAM software,
- 4) to input the parameters and the constraints in the part model, and
- 5) to change the part by assigning different parameter values.

In the conventional part modeling method, all part dimensions have to be defined independently, and they are specified with the design data. To change a part dimension, the dimension has to be found manually and then a new value is assigned. The conventional method is time-consuming and arduous, and some CAD/CAM software now is still using this method. Fortunately, some major CAD/CAM software, such as CATIA V5, Pro/E Wildfire, and Siemens NX, now has the parametric modeling function. In the software, the feature parameters and the geometric and dimensional constraints can be specified. The parameter values of a part design can be automatically assigned to the parameters of the CAD model with a spread sheet, macro script, or by manually changing the parameter values. The solid CAD model of the part can be quickly modified and updated so that it can be used for analysis.

1.4 Area Moment of Inertia

The area moment of inertia is the second moment of area around a given axis. Its definition is $I_x = \int y^2 \cdot dA$, when the section is symmetrical about the x or y axis. When this is not the case, the area moment of inertia around the y axis, I_y , and the product moment of area, I_{xy} , are required to obtain different area moment of inertia around different axis. It is a property of a sectional shape that is used to measure the resistance to bending and deflection. The SI unit of the second moment of area is m^4 .

For accurate CNC machining, we need to calculate area moments of inertia of end-mills to predict machined errors and to simulate machined surfaces. Prediction accuracy and simulation results are depend on how accurate the moments of inertia are. Until now, the area moment of inertia of a cutting tool is still approximated as a cantilevered beam with an effective radius as 80% of the radius of the cutting tool. But in an actual cutting tool, with different cutting flutes, the section of the cutting tool may not be a symmetrical shape. For example, a two-flute cutting tool is not a symmetrical one, but the other end-mills are. Their deflections caused by the cutting tool in a different axis direction are different.

1.5 Literature Review

Many technical articles have discussed about the generalized models of cutting tools, including the mathematical and manufacturing models [1-9]. Engin and Altintas [1] described a mathematical model of general end-mills often used in the industry. The end-mill geometry was modeled with flutes along the helical cutting edge. Chen et al. [2] presented a comprehensive manufacturing model that can be used to produce a concave cone end-mill on a 2-axis NC machine. Based on the design parameters and criteria, the equations of the flute and the cutting edge were derived. Chen et al. [3] provided a method for manufacturing concave-arc ball-end cutters using a 2-axis NC machine. The models that are used to calculate the actually obtained flutes and the computer simulation method were introduced. Wang et al. [4] established the geometrical and manufacturing models of

the rake face and the flank by introducing a sphere and helicoid model used to grind the rake face and the flank of the cutter. Chen and Lin [5] developed a systematic method that integrates design, manufacturing, simulation, and remedy. Based on the envelope condition, the approaches to solving the direct and inverse problems related to the manufacturing models were proposed. Lin and Lai [6] presented a mathematical model for a ball end-mill that can be used to design and manufacture by using a 2-axis NC machine. Tsai and Hsieh [7] proposed an analysis method that integrates design, manufacturing, and numerical simulation to obtain a model for the design and NC manufacturing of a ball end-mill. Furthermore, the helical cutting edge, the flute profile, and the cross section of the grinding wheel were formulated. Chen and Chen [8] presented a mathematic model of the helical curve of the cutting edge and cutting flute, the design of the grinding wheels used in the NC machining of toroidal cutters with a concave-arc generator. Chen [9] built mathematical models to overcome the two major problems associated with the design and manufacturing of ball end-mills. The first problem was that the mathematical equation of the cutting edge on the hemi-sphere of a ball end-mill, while the second problem was related to the grinding wheel feeding speed. All the nine papers were focused on the NC manufacturing model and the envelope model with a cutting flute model. No CAD model of the cutting flute on the ball or the bull head has been developed. Liu and Chang [10] studied the design of hob cutters for generating cutting angles (the radial rake angle, the relief angle, and the clearance angel) of cutting tools on a hobing process. This paper discussed manufacturing processes using a hob instead of a grinding wheel.

In order to finish the objective of the thesis, which is parametric modeling of the end mills, three related papers are reviewed [11-13]. Sheth and Malkin [11] reviewed commercial CAD/CAM software for the design and manufacture of components with helical flutes. The CAD system could help engineers design the profile of the tool and the helical flute. Kaldor et al. [12] dealt with geometrical analysis and development for designing the cutter and the grinding wheel profile. The direct and the inverse methods allow prediction of the helical flute profile and the cutter profile, respectively. Kang et al. [13] proposed an analytical solution to helical flute machining through a CAD approach, and a generalized helical flute machining model using the principles of differential geometry and kinematics, was formulated. These papers covered cutter modeling with CAD software.

With regard to spline applications, three papers are reviewed [14-16]. Xu, et al. [14] generated spline tool paths to machine free-form surfaces. The paths could avoid inefficient five-axis machining by automatically creating and verifying feasible tool-paths prior to cutting. Yin [15] presented a CAD representation of a free-form surface from a point cloud with NURBS or B-spline, which can be described to generate progressive fitting and multi-resolution tool paths. Razavi and Milner [16] discussed some foundational concepts about free-surface applications for computer implementation, lofting techniques, or computer-aided design.

This thesis therefore will focus on a free-form CAD model design of the end mill using NURBS curves technique.

1.6 Objectives of the Thesis

The objective of this thesis is to build a parametric solid model of the fillet tapered end-mills with the CATIA V5 software, based on all free-form curves. According to the cutting tools from the modern industrial field, the features of the fillet tapered end-mills include several flutes which include the relief edge and the clearance edge, rake edge of the side cutting edges, the cutting edges, and the first and the second flank faces of the bottom cutting edges, the gash, and the neck. In this thesis, all the geometry features will be parameterized and their CATIA models will be constructed. Based on this model, their area moment of inertia will be calculated, some simulation applications for predicting cutting force will be represented.

1.7 Outline of the Thesis

This thesis comprises of seven chapters. Chapter one introduces some basic concepts of spline curve, parametric design, area moment of inertia, literature review and thesis objectives. Chapter two and three presents the free-form parametric representation of cutting edges and cutting flutes, respectively. Chapter four describes two calculation methods of area moment of inertia of cutters: one is based on the sectional flute model built in Chapter two and three; another one is related to the special parts, such as the gash and the neck. In Chapters five, some applications of model are presented, the analysis of the difference of cutter flutes between the presented models or calculated area moment of

inertia is provided. Chapter six describes the major work of this thesis and future work. In Chapter seven, some of the references are listed.

Chapter 2 Parametric Modeling of the Side Cutting Edge of the Flute

2.1 List of Nomenclature of the Parametric Model

Parameters	Definition
θ	Helical angle of the cutting edge of an end-mill
R_s	Radial distance between the fillet center and the cutter axis
R	Corner radius of an end-mill
L	Axial length of a cutter
α	Taper angle of an tapered end-mill
k	Order of Taylor's series
e	Distance error between two points
ξ	Tolerance for converting a Taylor's series into a B-spline curve
n	Number of polynomial pieces
P	Coordinates of control points
R_L	Maximum radial of cutting
$r(z)$	Radius of cutting
$\psi(z)$	Lag angle
H	Helical cutting edge
$L(z)$	Longitudinal line
$S(z, \psi)$	Tapered cutting surface
$S(\eta, \psi)$	Toroidal cutting surface
θ	Helical angle of the cutting edge of an end-mill
R_s	Radial distance between the fillet center and the cutter axis

2.2 Parametric Representation of the Cutting Surfaces

The cutting surface of a fillet tapered end-mill is shown in Fig 2.1, and it is defined with a group of parameters for the geometric features. Specifically, the lower part of the cutting surface is a toroidal surface with radius of R , and the upper part is a conic surface with the tapered angle of α and radius of R_L of the top circle. The toroidal surface is tangent to the conic surface. The fillet tapered end-mill is in generic shape; for α and R are zero, it becomes a flat end-mill, and for α and R_s are zero, it is a ball end-mill. Flat, ball, and fillet end-mills are popular cutters in milling.

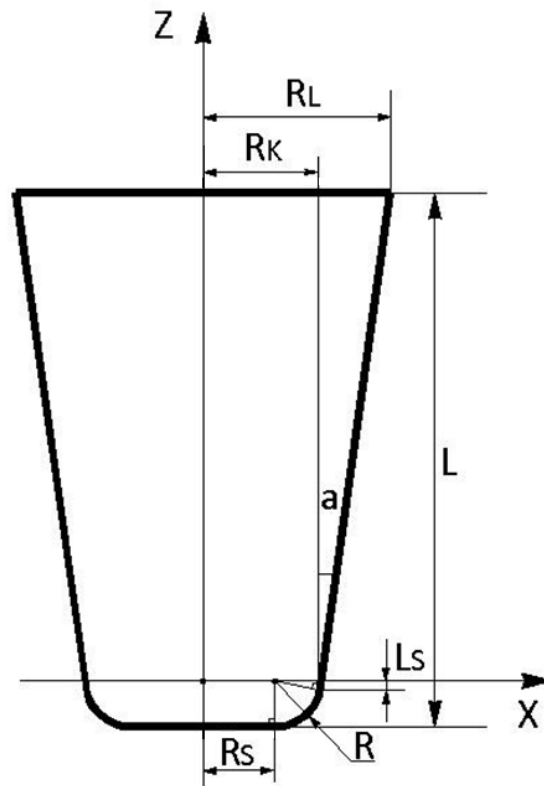


Figure 2.1. Illustration of a fillet tapered end-mill with parameters.

To represent the cutting surface geometry of the fillet tapered end-mill, a tool coordinate system (X-Y-Z) is built in the following way: the origin of the coordinate system is at point O, the Z-axis is the same with the cutter axis, and the X- and the Y-axes are located on the bottom plane perpendicular to the cutter axis (see Fig 2.1). In this coordinate system, the parametric equations of the geometric features of the cutting surface will be derived in the following sections.

2.2.1 Radius of the Toroidal Cutting Surface

The radius of the circle on a cross section z of the toroidal cutting surface is

$$r_1(z) = R_s + \sqrt{R^2 - z^2}, \quad (2.1)$$

where $-R < z \leq -L_s$ and $L_s = R \cdot \sin \alpha$.

2.2.2 Radius of the Conic Cutting Surface

The radius of the circle on a cross section z on the conic cutting surface is

$$r_2(z) = R_k + (z + L_s) \cdot \tan \alpha, \quad (2.2)$$

where $-R < z \leq L - L_s$ and $R_k = R_s + R \cdot \cos \alpha$.

2.2.3 Parametric Equation of Cutting Surface

For the circle on a cross section, the central angle of a point is denoted as ϕ , starting from the X-axis. Since the circle can be represented with parameters, z and ϕ , a parametric equation of the cutting surface is

$$S(z, \phi) = \begin{bmatrix} r(z) \cdot \cos \phi \\ r(z) \cdot \sin \phi \\ z \end{bmatrix}, \quad (2.3)$$

where $-R \leq z \leq L - L_s$ and $0 \leq \phi < 2\pi$.

2.3 Differential Form of the Cutting Edge

Generally, a cutting edge of an end-mill is a helix curve on the cutting surface. In this work, the helical angle of the helix curve at a helix point is defined as the angle between the tangent vector to the helix at this point and the longitudinal curve of the cutting surface passing through this point. In this research, for helix curves on toroidal or conic cutting surfaces, the helical angles at all points on the curves are the same. However, based on the different requirement, the helical angles can also be defined the different at different points on the curves. Fig 2.2 defines a helical angle of a helix curve on a cutting surface.

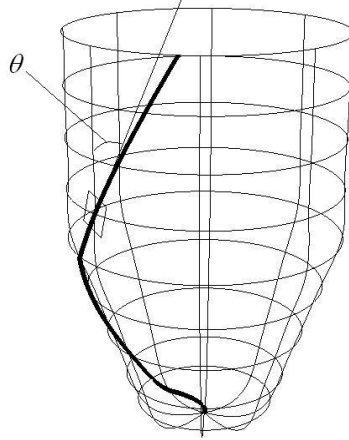


Figure 2.2. A helical angle of a helix curve on a cutting surface.

According to the definition of helical angle of a cutting edge, a parametric equation of cutting edge can be formulated. Assume a cross section intersects a cutting edge on the cutting surface at a point, the central angle measured from the X-axis is called lag angle $\psi(z)$. The lag angle changes along with the change of the Z coordinate of the cutting edge point. Thus, a cutting edge is denoted as $\mathbf{H}(z, \psi(z))$, and a lag angle of a point on a cutting edge is shown in Fig 2.3. The parametric equation of the helical cutting edge $\mathbf{H}(z)$ is

$$\mathbf{H}(z) = H(z, \psi(z)) = \begin{bmatrix} r(z) \cdot \cos(\psi(z)) \\ r(z) \cdot \sin(\psi(z)) \\ z \end{bmatrix}. \quad (2.4)$$

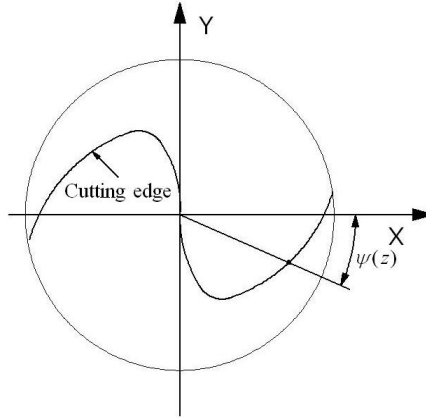


Figure 2.3. Illustration of a lag angle of a point on a cutting edge.

Due to variation of the radius on every surface, surfaces geometries and the helical cutting edges are different from each other. Meanwhile, using this invariable helical angle, the parametric equations of cutting edge can also be derived.

2.3.1 Helical Cutting Edge of the Toroidal Cutting Surface

For a helical cutting edge $\mathbf{H}_1(z)$ on the toroidal cutting surface, its lag angle is denoted as $\psi_1(z)$, which is a function of the cutting edge parameter z . The parametric equation of this helical cutting edge is

$$\mathbf{H}_1(z) = \begin{bmatrix} \left(R_s + \sqrt{R^2 - z^2} \right) \cdot \cos \psi_1 \\ \left(R_s + \sqrt{R^2 - z^2} \right) \cdot \sin \psi_1 \\ z \end{bmatrix}, \quad (2.5)$$

where $\psi_1 = \psi_1(z)$. The tangent vector of this helical curve is the first derivative of $\mathbf{H}_1(z)$ in terms of z ,

$$\frac{d\mathbf{H}_1}{dz} = \frac{d\mathbf{H}_1(z, \psi_1)}{dz} = \frac{\partial \mathbf{H}_1}{\partial z} + \frac{\partial \mathbf{H}_1}{\partial \psi_1} \cdot \frac{d\psi_1}{dz}. \quad (2.6)$$

Hence, the differential 1-form of the helical cutting edge $d\mathbf{H}_1$ can be represented as

$$d\mathbf{H}_1(z) = \frac{\partial \mathbf{H}_1}{\partial z} \cdot dz + \frac{\partial \mathbf{H}_1}{\partial \psi_1} \cdot d\psi_1, \quad (2.7)$$

where $\frac{\partial \mathbf{H}_1}{\partial z} = \begin{bmatrix} -\frac{z}{\sqrt{R^2 - z^2}} \cdot \cos \psi_1 \\ -\frac{z}{\sqrt{R^2 - z^2}} \cdot \sin \psi_1 \\ 1 \end{bmatrix}$, and $\frac{\partial \mathbf{H}_1}{\partial \psi_1} = \begin{bmatrix} -(R_s + \sqrt{R^2 - z^2}) \cdot \sin \psi_1 \\ (R_s + \sqrt{R^2 - z^2}) \cdot \cos \psi_1 \\ 0 \end{bmatrix}$.

Thus, the following two equations can be attained.

$$d\mathbf{H}_1(z) = \begin{bmatrix} -\frac{z}{\sqrt{R^2 - z^2}} \cdot \cos \psi_1 \cdot dz - (R_s + \sqrt{R^2 - z^2}) \cdot \sin \psi_1 \cdot d\psi_1 \\ -\frac{z}{\sqrt{R^2 - z^2}} \cdot \sin \psi_1 \cdot dz + (R_s + \sqrt{R^2 - z^2}) \cdot \cos \psi_1 \cdot d\psi_1 \\ dz \end{bmatrix}, \quad (2.8)$$

and

$$|d\mathbf{H}_1(z)|^2 = \frac{R^2 \cdot dz^2}{R^2 - z^2} + (R_s + \sqrt{R^2 - z^2})^2 \cdot d\psi_1^2.$$

A longitudinal curve of the toroidal surface is on the cutting surface and with a constant lag angle, which is independent on the parameter z . Here, a parametric equation of a

longitudinal line on the toroidal cutting surface is denoted as $\mathbf{L}_1(z)$. Thus, it can be represented with the parametric equation of the cutting surface with a fixed lag angle ψ_1 ,

$$\mathbf{L}_1(z) = \mathbf{S}_1(z, \psi_1) = \begin{bmatrix} r_1(z) \cdot \cos \psi_1 \\ r_1(z) \cdot \sin \psi_1 \\ z \end{bmatrix}, \quad (2.9)$$

where $-R \leq z \leq -L_s$. The tangent vector of the longitudinal curve is the first derivative of $\mathbf{L}_1(z)$ in terms of z , which is equal to the first derivative of $\mathbf{S}_1(z)$ in terms of z ,

$$\frac{d\mathbf{L}_1}{dz} = \frac{\partial \mathbf{S}_1}{\partial z}. \quad (2.10)$$

So, the differential 1-form of the tangential vector $d\mathbf{L}_1(z)$ of the longitudinal line is

$$d\mathbf{L}_1(z) = \frac{\partial \mathbf{S}_1}{\partial z} \cdot dz = \begin{bmatrix} \frac{-z}{\sqrt{R^2 - z^2}} \cdot \cos \psi_1 \cdot dz \\ \frac{-z}{\sqrt{R^2 - z^2}} \cdot \sin \psi_1 \cdot dz \\ dz \end{bmatrix}, \quad (2.11)$$

$$\text{so } |d\mathbf{L}_1(z)| = \frac{R \cdot dz}{\sqrt{R^2 - z^2}}.$$

By referring to the helix definition, the helical angle θ is between the tangent vectors $d\mathbf{L}_1(z)$ and $d\mathbf{H}_1(z)$, which can be expressed with the following equation.

$$\cos \theta = \frac{d\mathbf{H}_1 \cdot d\mathbf{L}_1}{|d\mathbf{H}_1| \cdot |d\mathbf{L}_1|}. \quad (2.12)$$

For a right-hand helix cutting edge, the differential 1-form of the lag angle of ψ_1 relation to z on the toroidal surface can be found as

$$d\psi_1 = \frac{\tan\theta \cdot R}{\left(R_s + \sqrt{R^2 - z^2}\right) \cdot \sqrt{R^2 - z^2}} \cdot dz. \quad (2.13)$$

2.3.2 Helical Cutting Edge of the Conic Cutting Surface

For a helical curve $\mathbf{H}_2(z)$ of the conic cutting surface with the lag angle $\psi_2(z)$, it can be represented as

$$\mathbf{H}_2(z) = \begin{bmatrix} \left(R_k + (z + L_s) \cdot \tan\alpha\right) \cdot \cos(\psi_2(z)) \\ \left(R_k + (z + L_s) \cdot \tan\alpha\right) \cdot \sin(\psi_2(z)) \\ z \end{bmatrix}. \quad (2.14)$$

The tangent vector of the helical curve is the first derivative of $\mathbf{H}_2(z)$ in terms of z , which is represented as

$$\frac{d\mathbf{H}_2}{dz} = \frac{d\mathbf{S}_2(z, \psi_2)}{dz} = \frac{\partial \mathbf{S}_2}{\partial z} + \frac{\partial \mathbf{S}_2}{\partial \psi_2} \cdot \frac{d\psi_2}{dz}. \quad (2.15)$$

Hence, the differential 1-form of the tangential vector $d\mathbf{H}_2$ is found in the following equation,

$$d\mathbf{H}_2(z) = \frac{\partial \mathbf{S}_2}{\partial z} \cdot dz + \frac{\partial \mathbf{S}_2}{\partial \psi_2} \cdot d\psi_2, \quad (2.16)$$

where

$$\frac{\partial \mathbf{S}_2}{\partial z} = \begin{bmatrix} \tan \alpha \cdot \cos \psi_2 \\ \tan \alpha \cdot \sin \psi_2 \\ 1 \end{bmatrix}, \text{ and } \frac{\partial \mathbf{S}_2}{\partial \psi_2} = \begin{bmatrix} -(R_K + (z + L_S) \cdot \tan \alpha) \cdot \sin \psi_2 \\ (R_K + (z + L_S) \cdot \tan \alpha) \cdot \cos \psi_2 \\ 0 \end{bmatrix}. \quad (2.17)$$

Thus, the differential 1-form can be derived as

$$d\mathbf{H}_2(z) = \begin{bmatrix} \tan \alpha \cdot \cos \psi_2 \cdot dz - (R_K + (z + L_S) \cdot \tan \alpha) \cdot \sin \psi_2 \cdot d\psi_2 \\ \tan \alpha \cdot \sin \psi_2 \cdot dz + (R_K + (z + L_S) \cdot \tan \alpha) \cdot \cos \psi_2 \cdot d\psi_2 \\ dz \end{bmatrix}, \quad (2.18)$$

$$\text{and } |d\mathbf{H}_2(z)|^2 = \frac{dz^2}{\cos^2 \alpha} + (R_K + (z + L_S) \cdot \tan \alpha)^2 \cdot d\psi_2^2.$$

A longitudinal line of the conic cutting surface is a curve on the surface with a constant lag angle, independent of the parameter z . Thus, the parametric equation of the longitudinal line on the conic cutting surface $\mathbf{L}_2(z)$ can be represented as

$$\mathbf{L}_2(z) = \mathbf{S}_2(z, \psi_2) = \begin{bmatrix} r_2(z) \cdot \cos \psi_2 \\ r_2(z) \cdot \sin \psi_2 \\ z \end{bmatrix}, \text{ and } -L_S \leq z \leq L - L_S. \quad (2.19)$$

The tangent vector of the longitudinal line is the first derivative of $\mathbf{L}_2(z)$ in terms of z , which is equal to the first derivative of $\mathbf{S}_2(z)$ in terms of z ,

$$\frac{d\mathbf{L}_2}{dz} = \frac{\partial \mathbf{S}_2}{\partial z}. \quad (2.20)$$

So, the differential 1-form of the tangent vector is expressed as

$$d\mathbf{L}_2(z) = \frac{\partial \mathbf{S}_2}{\partial z} \cdot dz = \begin{bmatrix} \tan \alpha \cdot \cos \psi_2 \cdot dz \\ \tan \alpha \cdot \sin \psi_2 \cdot dz \\ dz \end{bmatrix}, \quad (2.21)$$

and $|d\mathbf{L}_2(z)| = \frac{dz}{\cos \alpha}$.

By referring to the helix definition, the helical angle θ is between the tangent vectors $d\mathbf{L}_2(z)$ and $d\mathbf{H}_2(z)$, which can be expressed with the following equation,

$$\cos \theta = \frac{d\mathbf{H}_2 \cdot d\mathbf{L}_2}{|d\mathbf{H}_2| \cdot |d\mathbf{L}_2|}. \quad (2.22)$$

For a right-hand helix curve cutting edge, the differential 1-form of the lag angle ψ_2 in relation to z is derived as

$$d\psi_2 = \frac{\tan \theta}{(R_k + (z + L_s) \cdot \tan \alpha) \cdot \cos \alpha} \cdot dz. \quad (2.23)$$

2.4 Explicit Equation of the Lag Angle of the Cutting Edge

2.4.1 Lag Angle of the Cutting Edge of the Toroidal Cutting Surface

To attain an explicit formula of the cutting edge, the lag angle should be represented in an explicit form. Based on the above differential 1-form of the lag angle ψ_1 on the toroidal cutting surface, the equation of the lag angle is found by integrating its differential form. For clarity, the differential 1-form of the lag angle ψ_1 is repeated here,

$$d\psi_1 = \frac{\tan\theta \cdot R}{\left(R_s + \sqrt{R^2 - z^2}\right) \cdot \sqrt{R^2 - z^2}} \cdot dz, \quad (2.24)$$

where $-R < z \leq -L_s$. Here, let $z = R \cdot \sin\eta$,

$$d\psi_1 = \tan\theta \cdot R \cdot \frac{1}{R_s + R \cdot \cos\eta} \cdot d\eta. \quad (2.25)$$

By integrating, the lag angle equation is found,

$$\psi_1(\eta) = \frac{\tan\theta \cdot R}{R_s \cdot \sin\bar{\beta}} \cdot \left[2 \cdot \tan^{-1} \left(\tan \frac{\bar{\beta}}{2} \cdot \tan \frac{\eta}{2} \right) + C_1 \right], \quad (2.26)$$

where $\bar{\beta} = \cos^{-1} \left(\frac{R}{R_s} \right)$ and $z = R \cdot \sin\eta$. For the boundary conditions of the cutting edge, it

starts from the bottom of the cutter, which means when $z_{1s} = -R$ and $\eta = -\frac{\pi}{2}$, the lag angle should be zero. They are expressed as

$$\psi_{1s} = \psi_1 \Big|_{z=-R} = 0,$$

and

$$\psi_1(\eta) = \frac{\tan\theta \cdot R}{R_s \cdot \sin\bar{\beta}} \cdot \left[-2 \cdot \tan^{-1} \left(\tan \frac{\bar{\beta}}{2} \cdot \tan \frac{\pi}{4} \right) + C_1 \right] = 0.$$

Thus, the constant C_1 can be determined as

$$C_1 = \bar{\beta}.$$

Therefore, the explicit equation of the lag angle of the cutting edge on the toroidal cutting surface is

$$\psi_1(\eta) = \frac{\tan\theta \cdot R}{R_s \cdot \sin\bar{\beta}} \cdot \left[2 \cdot \tan^{-1} \left(\tan \frac{\bar{\beta}}{2} \cdot \tan \frac{\eta}{2} \right) + \bar{\beta} \right]. \quad (2.27)$$

The lag angle of the end point of the cutting edge is

$$\psi_{1e} = \psi_1(\eta) \Big|_{\eta = -\sin^{-1}(L_s/R)}.$$

Based on this equation, the lag angle of any point on the cutting edge on the toroidal cutting surface can be calculated. Consequently, the coordinates of any point on the helix cutting edge can be calculated.

Based on the cutting edge equation, by replacing the parameter z with η , the equation of the cutting edge on the toroidal cutting surface is simplified as

$$\mathbf{H}_1(\eta) = \begin{bmatrix} (R_s + R \cdot \cos \eta) \cdot \cos \left(\frac{\tan \theta \cdot R}{R_s \cdot \sin \beta} \cdot \left[2 \cdot \tan^{-1} \left(\tan \frac{\bar{\beta}}{2} \cdot \tan \frac{\eta}{2} \right) + \bar{\beta} \right] \right) \\ (R_s + R \cdot \cos \eta) \cdot \sin \left(\frac{\tan \theta \cdot R}{R_s \cdot \sin \beta} \cdot \left[2 \cdot \tan^{-1} \left(\tan \frac{\bar{\beta}}{2} \cdot \tan \frac{\eta}{2} \right) + \bar{\beta} \right] \right) \\ R \cdot \sin \eta \end{bmatrix}, \quad (2.28)$$

where $-\frac{\pi}{2} \leq \eta \leq -\sin^{-1} \left(\frac{L_s}{R} \right)$.

2.4.2 Lag Angle of the Cutting Edge of the Conic Cutting Surface

Similar to the way of finding the explicit equation of the lag angle of the cutting edge on the toroidal cutting surface, the equation of the lag angle of the cutting edge on the conic cutting surface is derived in this section. For clarity, the differential 1-form of the lag angle ψ_2 of the cutting edge on the conic cutting surface is repeated here,

$$d\psi_2 = \frac{\tan \theta}{(R_k + (z + L_s) \cdot \tan \alpha) \cdot \cos \alpha} \cdot dz, \quad (2.29)$$

where $-L_s \leq z \leq L$. By integrating the above equation, the lag angle equation is

$$\psi_2(z) = \frac{\tan \theta}{\sin \alpha} \cdot \ln(R_k + (z + L_s) \cdot \tan \alpha) + C_2,$$

and $-L_s \leq z \leq L$. For the boundary conditions, the cutting edge starts at $z_{2s} = -L_s$, so the lag angle is equal to ψ_{1e}

$$\psi_{2s} = \psi_{1e} \Big|_{z=-L_s},$$

and

$$\psi_2(z) = \frac{\tan\theta}{\sin\alpha} \cdot \ln(R_K + (z + L_s) \cdot \tan\alpha) + C_2 = \psi_{1e},$$

Thus, the constant C_2 is determined as

$$C_2 = \psi_{1e} - \frac{\tan\theta}{\sin\alpha} \cdot \ln(R_K).$$

Therefore, the explicit equation of the lag angle of the cutting edge on the conic cutting surface is

$$\psi_2(z) = \frac{\tan\theta}{\sin\alpha} \cdot \ln(R_K + (z + L_s) \cdot \tan\alpha) + \psi_{1e} - \frac{\tan\theta}{\sin\alpha} \cdot \ln(R_K). \quad (2.30)$$

Now, any point of the cutting edge on the conic cutting surface can be found. The cutting edge can be represented with a number of points calculated with the above equations. The explicit equation of the cutting edge on the conic cutting surface is

$$\mathbf{H}_2(z) = \begin{bmatrix} (R_K + (z + L_s) \cdot \tan\alpha) \cdot \cos\left(\frac{\tan\theta}{\sin\alpha} \cdot \ln(R_K + (z + L_s) \cdot \tan\alpha) + \psi_{1e} - \frac{\tan\theta}{\sin\alpha} \cdot \ln(R_K)\right) \\ (R_K + (z + L_s) \cdot \tan\alpha) \cdot \sin\left(\frac{\tan\theta}{\sin\alpha} \cdot \ln(R_K + (z + L_s) \cdot \tan\alpha) + \psi_{1e} - \frac{\tan\theta}{\sin\alpha} \cdot \ln(R_K)\right) \\ z \end{bmatrix}, \quad (2.31)$$

where $-L_s \leq z \leq L - L_s$.

2.5 Cutting Edge Representation with a B-Spline

2.5.1 Cutting Edge Representation with a Taylor's Series

To construct a helical cutting edge of a cutter in its solid model with CATIA V5 R20, an effective way is to convert the analytical equation of the cutting edge into a B-spline within a prescribed tolerance and then to input the B-spline into CATIA to generate the cutting edge using the spline function available in CATIA. In the previous sections, the analytical parametric equations of the helical cutting edge were derived; unfortunately, these equations cannot be directly applied to CATIA. To address this problem in my work, an effective solution is proposed to convert the analytical equation of the cutting edge using a number of Taylor's series, which are polynomials, and then to convert the Taylor's series into B-spline curves. Eventually, the B-spline curves are imported into CATIA as the model of the helical cutting edge. A conventional way of representing the cutting edge using its analytical equation is to sample a large number of points on the cutting edge by calculating their coordinates with the equation and then to feed these points into CATIA. Compared to this method, the newly proposed method in my work is more accurate with the least amount of data in representing the helical cutting edge.

First, the aforesaid analytical equations of the cutting edges on the toroidal and the conic cutting surface are converted into two Taylor's series within a prescribed tolerance ε . The reason for this is that the analytical forms are not polynomials, and they cannot be directly

converted into B-splines. A Taylor's series can accurately represent the neighbourhood of a function at a certain point, and, mathematically, it is the sum of an infinite number of terms including different derivatives and powers at the point. In practice, a finite number k of terms are used, for example, five to seven terms, for high accuracy and high efficiency. The generic equation of a Taylor's series at a break point $x_i = a$ is

$$f(x) = \sum_{n=0}^{\infty} \frac{f^{(n)}(a)}{n!} (x-a)^n. \quad (2.32)$$

For the analytical equations of the cutting edges, they are simply denoted as

$$\mathbf{H}(\nu) = \begin{bmatrix} x(\nu) \\ y(\nu) \\ z(\nu) \end{bmatrix},$$

where $\nu = \eta$ for the cutting edge on the toroidal surface and $\nu = z$ for the cutting edge on the conic surface of the cutter. Assume the first break is selected at b_1 and the maximum degree of all the terms is k , the first Taylor's series at the first break is

$$\mathbf{T}_1(\nu) = \begin{bmatrix} x_1^T(\nu) \\ y_1^T(\nu) \\ z_1^T(\nu) \end{bmatrix} = \begin{bmatrix} x(b_1) + \frac{dx(b_1)}{1!} \cdot (\nu - b_1) + \frac{dx^{(2)}(b_1)}{2!} \cdot (\nu - b_1)^2 + \dots + \frac{dx^{(k)}(b_1)}{k!} \cdot (\nu - b_1)^k \\ y(b_1) + \frac{dy(b_1)}{1!} \cdot (\nu - b_1) + \frac{dy^{(2)}(b_1)}{2!} \cdot (\nu - b_1)^2 + \dots + \frac{dy^{(k)}(b_1)}{k!} \cdot (\nu - b_1)^k \\ z(b_1) + \frac{dz(b_1)}{1!} \cdot (\nu - b_1) + \frac{dz^{(2)}(b_1)}{2!} \cdot (\nu - b_1)^2 + \dots + \frac{dz^{(k)}(b_1)}{k!} \cdot (\nu - b_1)^k \end{bmatrix}. \quad (2.33)$$

By changing the parameter ν in its domain, the deviation between the Taylor's series and the analytical cutting edge equation can be formulated as

$$e(\nu) = \sqrt{(x(\nu) - x_1^T(\nu))^2 + (y(\nu) - y_1^T(\nu))^2 + (z(\nu) - z_1^T(\nu))^2}. \quad (2.34)$$

To ensure the accuracy of the Taylor's series with regard to the analytic cutting edge equation, the maximum derivation between them should be equal to the specified tolerance ε . The constraint of the conversion is expressed as

$$e_{\max}(v) = \sqrt{\left(x(v_{\max}) - x_1^T(v_{\max})\right)^2 + \left(y(v_{\max}) - y_1^T(v_{\max})\right)^2 + \left(z(v_{\max}) - z_1^T(v_{\max})\right)^2} \leq \varepsilon.$$

After finding the maximum value of v subject to the constraint, the first Taylor's series is found, and v_{\max} is taken as the new break point for the second Taylor's series. With the same procedure, a number of Taylor's series are found, and the whole cutting edges on the toroidal and the conic cutting surfaces are represented with the Taylor's series. For each Taylor's series $\mathbf{T}_i(v)$ at a break b_i , it can be formulated as

$$\mathbf{T}_i(v) = \begin{bmatrix} x_i^T(v) \\ y_i^T(v) \\ z_i^T(v) \end{bmatrix} = \begin{bmatrix} x(b_i) + \frac{dx(b_i)}{1!} \cdot (v - b_i) + \frac{dx^{(2)}(b_i)}{2!} \cdot (v - b_i)^2 + \dots + \frac{dx^{(k)}(b_i)}{k!} \cdot (v - b_i)^k \\ y(b_i) + \frac{dy(b_i)}{1!} \cdot (v - b_i) + \frac{dy^{(2)}(b_i)}{2!} \cdot (v - b_i)^2 + \dots + \frac{dy^{(k)}(b_i)}{k!} \cdot (v - b_i)^k \\ z(b_i) + \frac{dz(b_i)}{1!} \cdot (v - b_i) + \frac{dz^{(2)}(b_i)}{2!} \cdot (v - b_i)^2 + \dots + \frac{dz^{(k)}(b_i)}{k!} \cdot (v - b_i)^k \end{bmatrix}. \quad (2.35)$$

where $v > b_i$. The Taylor's series is found when the deviation between it and the cutting edge in analytical form. Finally, a number n of Taylor's series are found, which are n polynomials as $\mathbf{T}_1, \mathbf{T}_2, \dots, \mathbf{T}_n$, and the Taylor's series will be converted into B-splines.

2.5.2 Conversion of Taylor's Series to B-Splines

In the previous section, the helical cutting edges on the toroidal and the conic cutting surfaces are now represented with a number of Taylor's series. The Taylor's series actually are piecewise polynomials, and the B-splines mathematically are piecewise polynomials.

The method of converting piecewise polynomials into B-splines is well established. In this section, assuming a number of (n) Taylor's series are found for the cutting edges and the order of the Taylor's series is k . Each polynomial is converted into a B-spline, whose order is five. A B-spline curve is represented as

$$\mathbf{P}_i(\mathbf{v}) = \sum_{j=0}^5 (N_{j,5}(\mathbf{v}) \cdot \mathbf{P}_{i,j}), \quad (2.36)$$

where $\mathbf{v} \in [b_1, b_n]$. The blending function is defined as

$$N_{j,k}(\mathbf{v}) = \frac{(\mathbf{v} - t_j) \cdot N_{j,k-1}(\mathbf{v})}{t_{j+k-1} - t_j} + \frac{(t_{j+k} - \mathbf{v}) \cdot N_{j+1,k-1}(\mathbf{v})}{t_{j+k} - t_{j+1}}. \quad (2.37)$$

The knots of B-spline are defined as

$$t = [b_1, b_1, b_1, b_1, b_1, b_2, b_2, b_2, b_2, b_2, \dots, b_{n+1}, b_{n+1}, b_{n+1}]. \quad (2.38)$$

By using the function `fm2fn` in MATLAB, each Taylor's series is converted into a B-spline curve, where the `fm2fn` is a function to convert a piecewise polynomial into a B-spline curve.

2.6 Application and Analysis

In this section, the mathematical background of converting the analytical equation of the cutting edge into B-spline representation is elaborated. To demonstrate the process of the conversion, this method is applied to a solid carbide fillet tapered end-mill. The parameter values of the tool are listed in Tab 2.1, and the tool model is shown in Fig 2.4.

Table 2.1 The parameter values of a solid carbide fillet tapered end-mill.

R_S mm	R mm	L mm	R_L mm	R_K mm	L_S mm	α deg.	θ deg.
7	3	40	12.6	10	0.2	4	40

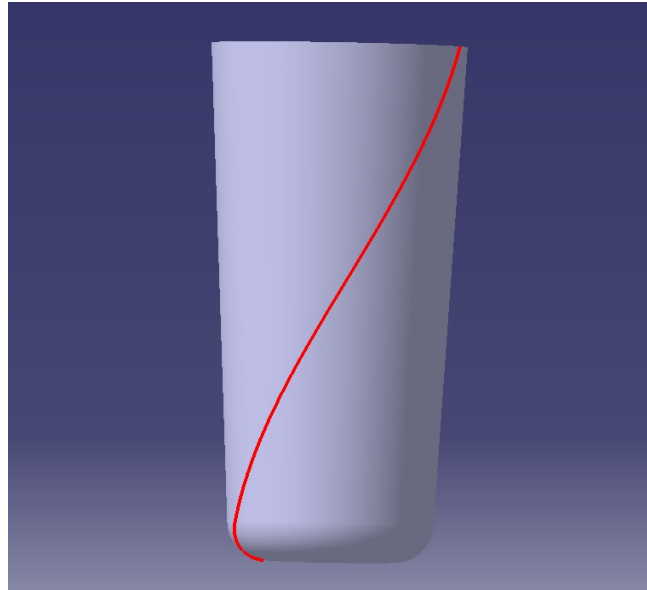


Figure 2.2. A helical cutting edge on the cutting surface of a solid carbide fillet tapered end-mills in CATIA.

Based on the parameters of the tool and the cutting edge, the analytical equations of the cutting edges on the toroidal and the conic cutting surfaces are found. The analytical equations are converted in a number of Taylor's series within different tolerances, and then the Taylor's series are re-represented with B-splines. The numbers of Taylor's series on the toroidal and the conic surfaces are listed, and the total numbers of control points of the B-spline curves are provided in Tab 2.2. It is clear that with the increase of the Taylor' series order, the fewer the Taylor's series, the fewer the control points of the B-spline curve.

Table 2.2. Results analysis of conversion of the analytical equation into B-splines.

Taylor's series order	Tolerance of converting to Taylor's series (mm)	Number of Taylor's series on toroidal surface	Number of Taylor's series on conic surface	Number of control points of B-splines
3	0.1	4	10	42
4		3	6	36
5		2	4	30
3	0.01	7	20	81
4		4	10	56
5		3	6	45
3	0.001	16	44	180
4		7	17	96
5		4	9	65
3	10^{-4}	34	94	384
4		12	30	168
5		6	14	100
3	10^{-5}	74	205	837
4		21	52	292
5		10	23	165

To demonstrate the advantage of this new method over the conventional method, which is finding a number of cutting edge points and fitting them with a B-spline in CATIA, a number of experiments are conducted and are provided in the following. In each experiment, a number of cutting edge points are sampled and imported into CATIA, and then the points are fitted with a B-spline curve in CATIA. By checking the deviations between the CATIA B-spline and the analytical cutting edge equation at 100 locations, the maximum of the deviations is found. In the new method, a tolerance of converting the analytical equation

into a Taylor's series is specified, and a B-spline curve is found to represent the cutting edge. The deviations between the converted B-spline and the analytical equation at 100 locations are computed, and the maximum error is found. Five experiments are conducted and the corresponding results are provided in Table 2.3. It is evident that the new conversion method is more accurate to the analytical cutting edge, compared to the CATIA method. The comparison of the accuracy of the new method and the conventional method is plotted in Fig 2.5.

Table 2.3. Comparison between the new conversion method and the conventional method.

Number of cutting edge points in CATIA	Number of control points of CATIA B-spline	Tolerance of converting to Taylor's series (mm)	Number of control points of B-spline in conversion	Error of CATIA B-spline (mm)	Error of converted B-spline (mm)
4	12	1.5	10	0.1783	0.1746
6	17	0.2	15	0.0219	0.0200
7	20	0.05	20	0.0095	0.0042
11	30	0.01	30	0.0016	0.0008
13	35	0.005	35	0.0009	0.0005

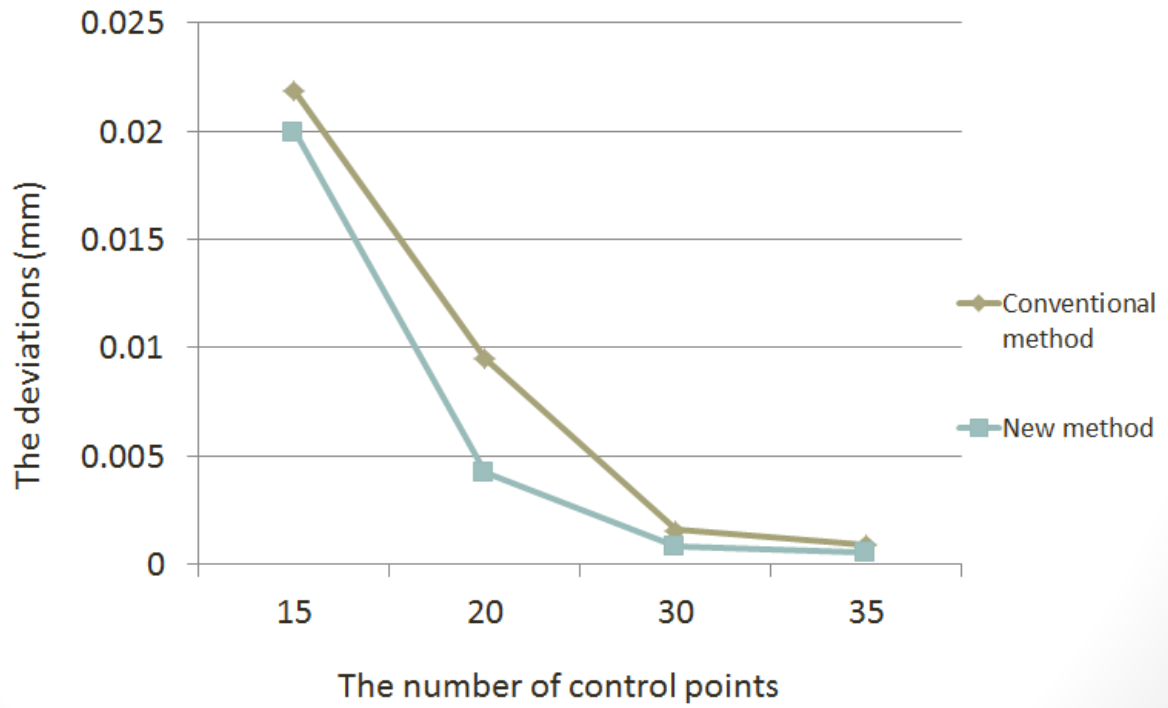


Figure 2.3. Comparison the accuracy between the new method and the conventional method using CATIA.

Chapter 3 Parametric Modeling of the Solid Cutter Flutes

3.1 List of Nomenclature of the Parametric Model

Parameters	Definition
n	Teeth (or flute) number of the cutter
α_1	Rake angle on the cutting flute cross-section
α_2	Relief angle on the cutting flute cross-section
α_3	Clearance angle on the cutting flute cross-section
l_{AB}	Length of the line AB on the cutting flute cross-section
l_{ED}	Length of the line ED on the cutting flute cross-section
l_{EF}	Length of the line EF on the cutting flute cross-section
P	Control points
r_o	Radius of core cutter
R_L	Radius of cutting
α_0	The angle between the tangent point of flute and center point with the x axis

3.2 Introduction

As a key feature, flutes of solid carbide end mills are also crucial to the cutter performance and life. Specifically, a flute geometrically includes a flute surface and a rake face. Thus, an end-mill's flutes determine the cutting forces and the core size that is very important to the

cutter rigidity; and, at the same time, they provide accommodation for chips and evacuate them during machining.

A flute profile is illustrated in Fig 3.1. Each section of the flute consists of four segments. The straight line AB, which forms a rake angle α_1 with the x axis, corresponds to the rake face. The NURBS BCD with eight control points is the section of the flute which blends the chip. The NURBS BCD is the section of the flute which removes the chip smoothly. Let the NURBS BCD pass C and be tangent to core at point C, on the same time, the NURBS BCD is tangent to the straight line AB at point B, and tangent to arc ED at point D. The straight line DE forms an angle α_3 with the tangential line at point F. The straight line EF, which forms a relief angle α_2 with the tangential line at point F, corresponds to the strip.

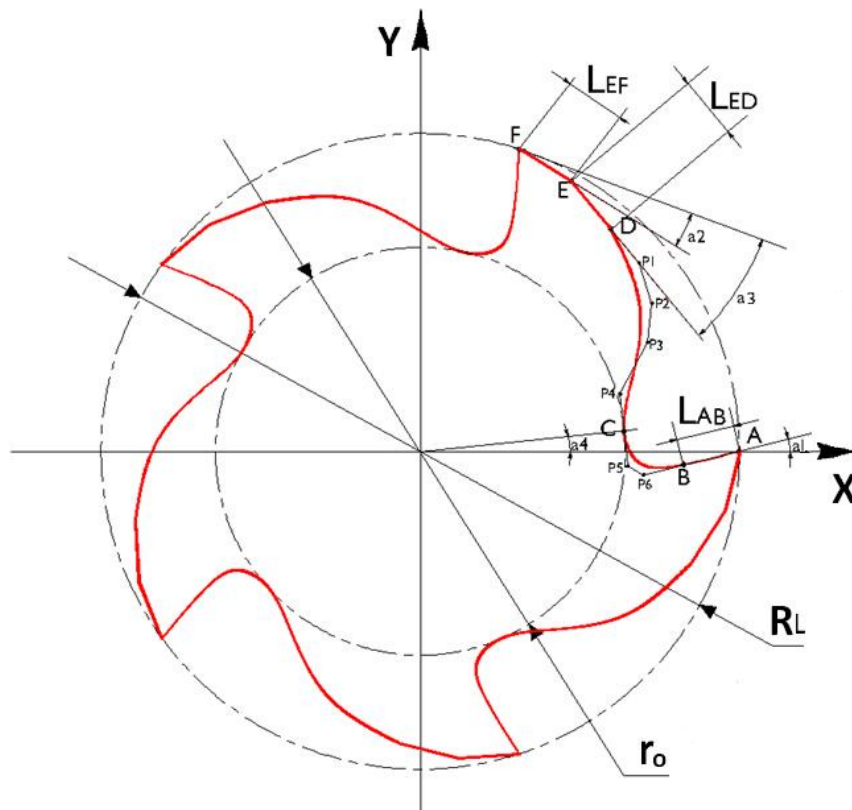


Figure 3.1. Sectional view of a cutting flute.

3.3 The Coordinates of the Intersection Points of Cutting Flute

Suppose an end mill cutter has n teeth and the profile of a flute starts at point A (a tooth tip) on the X-axis and ends at point F (a neighbouring tooth tip), as shown in Fig 3.1. In this section, the central angle between two adjacent teeth is called a teeth spacing angle, which is shown in Fig. 3.1 as ΔAOF , and a teeth spacing angle is equal to $2\pi/n$. The x- and y-coordinates of points A and F can be found in the tool coordinate system.

$$\mathbf{r}_A = \begin{bmatrix} x_A \\ y_A \end{bmatrix} = \begin{bmatrix} R_L \\ 0 \end{bmatrix},$$

and

$$\mathbf{r}_F = \begin{bmatrix} x_F \\ y_F \end{bmatrix} = \begin{bmatrix} R_L \cdot \cos\left(\frac{2\pi}{n}\right) \\ R_L \cdot \sin\left(\frac{2\pi}{n}\right) \end{bmatrix}. \quad (3.1)$$

The angle starting from the positive X-axis to line FE is denoted as ζ_{EF} , which can be found in terms of the relief angle α_2 , teeth spacing angle, and helical cutting edge direction. For a right-hand helical cutting edge,

$$\zeta_{FE} = \frac{2\pi}{n} - \frac{\pi}{2} - \alpha_2. \quad (3.2)$$

According to point F, the coordinate of point E is calculated as

$$\mathbf{r}_E = \begin{bmatrix} x_E \\ y_E \end{bmatrix} = \begin{bmatrix} x_F + l_{FE} \cdot \cos \zeta_{FE} \\ y_F + l_{FE} \cdot \sin \zeta_{FE} \end{bmatrix}. \quad (3.3)$$

Similarly, the angle starting from the positive X-axis to line ED is denoted as ζ_{ED} , and it can be formulated in terms of the clearance angle α_3 , teeth spacing angle, and helical cutting edge direction. For a right-hand cutting edge,

$$\zeta_{ED} = \frac{2\pi}{n} - \frac{\pi}{2} - \alpha_3. \quad (3.4)$$

The coordinate of point D is calculated as

$$\mathbf{r}_D = \begin{bmatrix} x_D \\ y_D \end{bmatrix} = \begin{bmatrix} x_E + l_{ED} \cdot \cos \zeta_{ED} \\ y_E + l_{ED} \cdot \sin \zeta_{ED} \end{bmatrix}. \quad (3.5)$$

Then, the coordinates of points B can be formulated as

$$\mathbf{r}_B = \begin{bmatrix} x_B \\ y_B \end{bmatrix} = \begin{bmatrix} x_A - l_{AB} \cdot \cos \alpha_1 \\ -l_{AB} \cdot \sin \alpha_1 \end{bmatrix}. \quad (3.6)$$

Finally, we set the coordinates of points C

$$\mathbf{r}_C = \begin{bmatrix} x_C \\ y_C \end{bmatrix} = \begin{bmatrix} r_0 \cdot \cos(\alpha_4) \\ r_0 \cdot \sin(\alpha_4) \end{bmatrix}. \quad (3.7)$$

Now, we set up six control points to make the section of the flute.

First, calculate three slopes of three lines

$$k_{ED} = \tan(\zeta_{ED}),$$

$$k_{AB} = \frac{y_A - y_B}{x_A - x_B},$$

$$k_C = -\frac{x_C}{y_C}.$$

and three constant of three lines function,

$$b_{ED} = y_E - k_{DE} \cdot x_E,$$

$$b_{AB} = y_A - k_{AB} \cdot x_A,$$

$$b_C = y_C - k_C \cdot x_C.$$

P1 should be on the extension of line ED,

$$P_1 = \begin{bmatrix} P_{1X} \\ P_{1Y} \end{bmatrix} = \begin{bmatrix} \text{user input} \\ k_{ED} \cdot P_{1X} + b_{ED} \end{bmatrix}. \quad (3.8)$$

P2 and P3 are input by user,

$$P_2 = \begin{bmatrix} P_{2X} \\ P_{2Y} \end{bmatrix} = \begin{bmatrix} \text{user input} \\ \text{user input} \end{bmatrix}, \quad (3.9)$$

and

$$P_3 = \begin{bmatrix} P_{3X} \\ P_{3Y} \end{bmatrix} = \begin{bmatrix} \text{user input} \\ \text{user input} \end{bmatrix}. \quad (3.10)$$

P4 and P5 should be on C line,

$$P_4 = \begin{bmatrix} P_{4X} \\ P_{4Y} \end{bmatrix} = \begin{bmatrix} \text{user input} \\ k_C \cdot P_{4X} + b_C \end{bmatrix}, \quad (3.11)$$

and

$$P_5 = \begin{bmatrix} P_{5X} \\ P_{5Y} \end{bmatrix} = \begin{bmatrix} \text{user input} \\ k_C \cdot P_{5X} + b_C \end{bmatrix}. \quad (3.12)$$

P6 should be on the extension of line AB,

$$P_6 = \begin{bmatrix} P_{6X} \\ P_{6Y} \end{bmatrix} = \begin{bmatrix} \text{user input} \\ k_{AB} \cdot P_{6X} + b_{AB} \end{bmatrix}. \quad (3.13)$$

For all the weights, users can define based on the geometry design.

$$w = [w1, w2, w3, w4, w5, w6]. \quad (3.14)$$

The spline flute is composed by following control points,

$$\begin{aligned} P(x, y) &= [P_x, P_y] \\ &= [A, B, C, D, E, F, P1, P2, P3, P4, P5, P6]. \end{aligned} \quad (3.15)$$

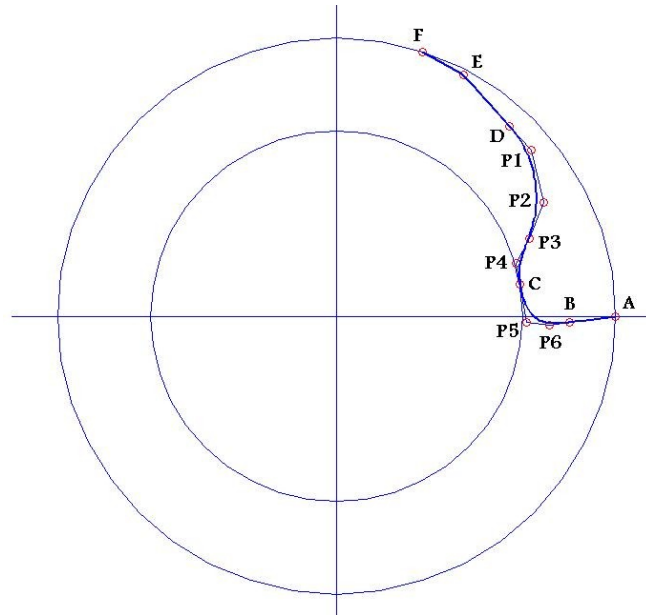


Figure 3.2. Diagram of the NURBS

We make it as a NURBS curve. In order to let this curve pass C point, we set degree as 4. We use 18 control points (in the segments AB, DE, EF, the control points will be repeated on E, D and B). The demonstration is shown in Fig 3.2.

Due to the number of control points n is 18, and take $k=4$, the knots $t[i]$ can be calculated

$$i \in \{1:(1+n+k)\},$$

when $i < (k+2)$

$$t[i] = 0,$$

when $i > (k+1) \& \& i < (n+1)$

$$t[i] = i - k - 1,$$

when $i < n$

$$t[i] = n - k,$$

$$t = [0 \ 0 \ 0 \ 0 \ 0 \ 1 \ 2 \ 3 \ 4 \ 5 \ 6 \ 7 \ 8 \ 9 \ 10 \ 11 \ 12 \ 13 \ 14 \ 14 \ 14 \ 14 \ 14].$$

The NURBS curve is represented

$$P(u) = \frac{\sum_{i=0}^n h_i P_i N_{i,k}(u)}{\sum_{i=0}^n h_i N_{i,k}(u)} = [P_x, P_y], \quad (3.16)$$

$$x \cdot h = \sum_{i=0}^n (h_i \cdot x_i) N_{i,k}(u),$$

$$y \cdot h = \sum_{i=0}^n (h_i \cdot y_i) N_{i,k}(u),$$

$$h = \sum_{i=0}^n (h_i) N_{i,k}(u),$$

$$N_{i,k}(u) = \frac{(u - t_i) \cdot N_{i,k-1}(u)}{t_{i+k-1} - t_i} + \frac{(t_{i+k} - u) \cdot N_{i+1,k-1}(u)}{t_{i+k} - t_{i+1}}, \quad (3.17)$$

$$u \in \{0, t(1+n+k)\}.$$

3.4 The 3D Models of Cutting Tools

Based on CATIA platform, the designed cutter flute can be swept along the two cutting edges as guide curve. Finally the solid carbide end mill can be generated. The demonstration is shown in Fig 3.3.

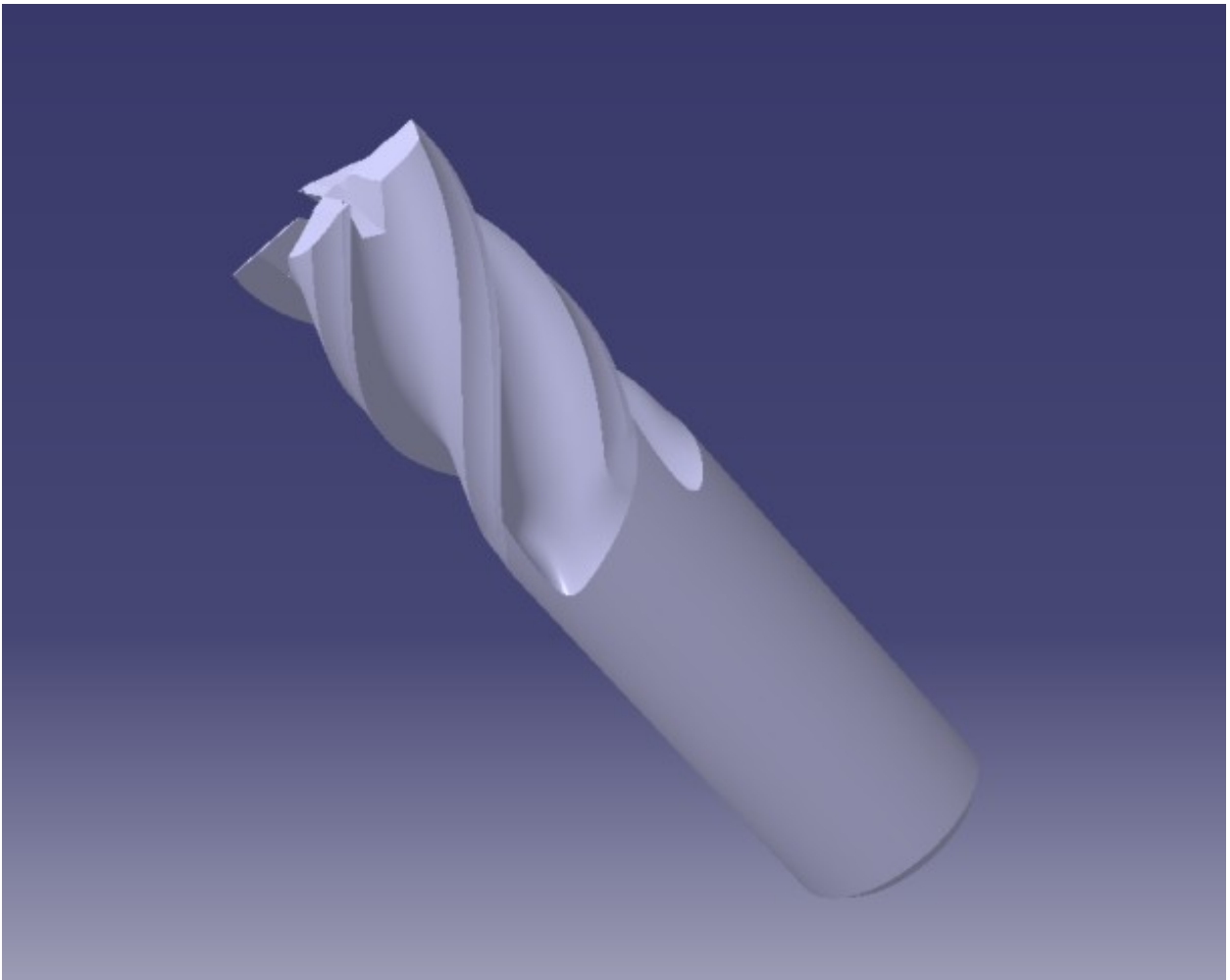


Figure 3.3. Illustration of solid carbide bull nose end mill.

Chapter 4 Area Moments of Inertia of Carbide Cutters

4.1 List of Notation and Introduction

Parameters	Definition
ΔL	The differential length
Δr	The differential thickness
n_t, t	The thickness scalar
n_l, l	The length scalar
S	The rotation scalar

In calculating the area moment of inertia, first of all, for side cutting edge of cutter, because the cross-section of cutter is the regular shape with function, one special method is represented. On every layer, every teeth can be separated into two portions, A (red) and B (blue). The result area moment of inertia is the difference between A and B. In each portion, all infinitesimal area and their coordinates can be calculated respectively, where all coordinates of portion B need to be rotated to portion B' to calculate. In portion A, the cutting flute is considered as infinitesimal scaled NURBS splines with the thickness Δr , and each infinitesimal scaled spline is divided into infinitesimal elements with an infinitesimal length ΔL . In portion B, due to the special shape, the cutting flute is divided into infinitesimal bands along x-axis with the thickness Δr , and each infinitesimal band is divided into infinitesimal elements with an infinitesimal height ΔL . By calculating all the area moment of inertia of these infinitesimal areas and adding them together, the area moment

of inertia of each spline can be obtained, and area moment of inertia of cutting flute can be obtained on every teeth. Finally add all area moment of inertia on all teeth to get the final area moment of inertia on each layer. The demonstration is shown in Fig 4.1, and this layer is taken as a reference one at $z=0$.

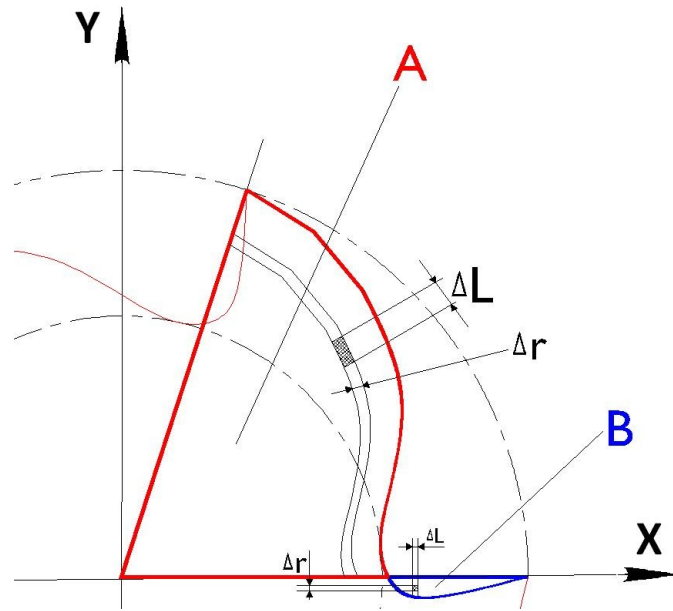


Figure 4.1. Illustration of the regular flute shape.

4.2 Representation of Splines

For every cutter teeth, the cutter flute is presented by one spline which can be scaled into n_l sections along this cutting flute, where we call n_l as the length scalar. Meantime, towards to cutter center axis, the cutter teeth layer can be scaled with n_t scaled splines with the infinitesimal thickness, where we call n_t as the thickness scalar. Moreover, all coordinates

of every scaled spline can also be obtained to calculate the length of every section. The control points of initial spline on this flute is

$$P(x,y)=[P_x,P_y],$$

It is a NURBS curve, with 18 control points (in the segments AB, DE, EF, the control points will be repeated), where degree is 4. This NURBS curve had been derived in Chapter Three. The demonstration is shown in Figs. 3.2.

The knots $t[i]$ is non-periodic uniform, which is,

$$t=[0\ 0\ 0\ 0\ 0\ 1\ 2\ 3\ 4\ 5\ 6\ 7\ 8\ 9\ 10\ 11\ 12\ 13\ 14\ 14\ 14\ 14\ 14],$$

NURBS curve is represented

$$P(u) = \frac{\sum_{i=0}^n h_i \cdot P_i \cdot N_{i,k}(u)}{\sum_{i=0}^n h_i \cdot N_{i,k}(u)} = [P_x, P_y],$$

$$N_{i,k}(u) = \frac{(u-t_i) \cdot N_{i,k-1}(u)}{t_{i+k-1} - t_i} + \frac{(t_{i+k} - u) \cdot N_{i+1,k-1}(u)}{t_{i+k} - t_{i+1}}$$

$$u \in \{0, t(1+n+k)\}.$$

4.3 Differential Method

The thickness scalar is

$$n_t = 100 ,$$

$$t \in \{1 : n_t\} .$$

The length scalar is

$$n_l = 1000 ,$$

$$l \in \{1 : n_l\} .$$

4.3.1 Portion A

The coordinates of the t th scaled spline are

$$P_t(u) = \frac{t}{n_t} \cdot P(u) ,$$

where u is the parameter of NURBS curve, and t is number of scaled NURBS curves .

The thickness Δr on every infinitesimal scaled spline is

$$\Delta r_{t,l} = \sqrt{\left(P_{t,l,x} - P_{(t-1),l,x}\right)^2 + \left(P_{t,l,y} - P_{(t-1),l,y}\right)^2} , \quad (4.1)$$

$$dr_l = \Delta r_l = \Delta r_{t,l} .$$

The calculation of the length of every spline

$$\Delta L_{t,l} = \sqrt{\left(P_{t,l,x} - P_{t,(l-1),x}\right)^2 + \left(P_{t,l,y} - P_{t,(l-1),y}\right)^2}. \quad (4.2)$$

In order to get the angle between $\Delta L_{t,l}$ and $\Delta r_{t,l}$, Δl_r can be used,

$$\Delta l_r = \sqrt{\left(P_{(t-1),l,x} - P_{t,(l-1),x}\right)^2 + \left(P_{(t-1),l,y} - P_{t,(l-1),y}\right)^2}, \quad (4.3)$$

The angle between $\Delta L_{t,l}$ and $\Delta r_{t,l}$ is l_r

$$\cos(l_r) = \frac{\left(\Delta L_{t,l}^2 + \Delta r_{t,l}^2 - \Delta l_r^2\right)}{2 \cdot \Delta r_{t,l} \cdot \Delta L_{t,l}},$$

$$\sin(l_r) = \sqrt{1 - \cos^2(l_r)}.$$

As the profile of one cutter flute changes, the infinitesimal length and thickness of each point on the spline of this profile will be represented in different formula. All these formulas can be deduced regarding to their profiles functions.

For one teeth of the first flute, the area moment of inertial can be calculated based on the below differential equations developed. Every infinitesimal area is enclosed by Δr and ΔL in this teeth profile.

$$dA = dr \cdot dL \cdot \sin(l_r) = \Delta r_{t,l} \cdot \Delta L_{t,l} \cdot \sin(l_r). \quad (4.4)$$

The area moment of inertia of each element around the x axis of each element is

$$dI_{A,t,l,x} = y^2 \cdot dA = P_y^2 \cdot dr \cdot dL \cdot \sin(l_r) = P_{t,l,y}^2 \cdot \Delta r_{t,l} \cdot \Delta L_{t,l} \cdot \sin(l_r). \quad (4.5)$$

The area moment of inertia of each element around the y axis of each element is

$$dI_{A,t,l,y} = x^2 \cdot dA = P_x^2 \cdot dr \cdot dL \cdot \sin(I_r) = P_{t,l,x}^2 \cdot \Delta r_{t,l} \cdot \Delta L_{t,l} \cdot \sin(I_r). \quad (4.6)$$

The product moment of area of each element is,

$$dI_{A,t,l,xy} = x \cdot y \cdot dA = P_x \cdot P_y \cdot dr \cdot dL \cdot \sin(I_r) = P_{t,l,x} \cdot P_{t,l,y} \cdot \Delta r_{t,l} \cdot \Delta L_{t,l} \cdot \sin(I_r). \quad (4.7)$$

4.3.2 Portion B

Only one spline is used

$$P_t(u) = P(u).$$

The thickness Δr on every infinitesimal band is

$$\Delta r = |P_x(u)_i - P_x(u)_{i-1}|, \quad (4.8)$$

$$dr_i = \Delta r.$$

The calculation of the length of every infinitesimal band is

$$\Delta L = \frac{|P_y(u)_i|}{n_i}. \quad (4.9)$$

For one teeth of the first flute, the area moment of inertial can be calculated based on the below differential equations developed. Every infinitesimal area is enclosed by Δr and ΔL in this teeth profile.

$$dA = dr \cdot dL = \Delta r \cdot \Delta L. \quad (4.10)$$

If the cutter has n tooth, the coordinates in portion B' be calculated by rotating an angle $2\pi/n$ from those in portion B.

$$P_{t,l,x} = P_x \cdot \cos\left(\frac{2 \cdot \pi}{n}\right) - P_y \cdot \sin\left(\frac{2 \cdot \pi}{n}\right)$$

$$P_{t,l,y} = P_x \cdot \sin\left(\frac{2 \cdot \pi}{n}\right) + P_y \cdot \cos\left(\frac{2 \cdot \pi}{n}\right)$$

The area moment of inertia of each element around the x axis of each element is

$$dl_{t,l,x} = y^2 \cdot dA = P_y^2 \cdot dr \cdot dL = P_{t,l,y}^2 \cdot \Delta r \cdot \Delta L . \quad (4.11)$$

The area moment of inertia of each element around the y axis of each element is

$$dl_{B,t,l,y} = x^2 \cdot dA = P_x^2 \cdot dr \cdot dL = P_{t,l,x}^2 \cdot \Delta r \cdot \Delta L . \quad (4.12)$$

The product moment of area of each element is,

$$dl_{B,t,l,xy} = x \cdot y \cdot dA = P_x \cdot P_y \cdot dr \cdot dL = P_{t,l,x} \cdot P_{t,l,y} \cdot \Delta r \cdot \Delta L . \quad (4.13)$$

4.4 Calculation of Area Moment of Inertia

By adding all the area moment of inertia around the x axis of each element in portion A, and subtracting all the area moment of inertia around the x axis of each element in portion B, the area moment of one certain spline around the x axis is calculated.

$$\Delta I_{t,x}^{nl} = \sum_{l=1}^{nl} (dl_{A,t,l,x} - dl_{B,t,l,x}) . \quad (4.14)$$

By adding all the area moment of inertia around the x axis of each spline, the area moment of inertia around the x axis of first flute is obtained.

$$I_x = \sum_{t=1}^{nt} \Delta I_{t-x}^{nl} .$$

The area moment of inertia around the y axis of one certain spline is obtained by adding all the area moment of inertia around the y axis of each element, and subtracting all the area moment of inertia around the x axis of each element in portion B,

$$\Delta I_{i,y}^{nl} = \sum_{l=1}^{nl} (dI_{A,t,l,y} - dI_{B,t,l,y}), \quad (4.15)$$

The area moment of inertia around the y axis of the first flute is calculated.

$$I_y = \sum_{t=1}^{nt} \Delta I_{t,y}^{nl}. \quad (4.16)$$

For the product moment of area of one certain band, by adding all the product moment of area of each element together, and subtracting all the area moment of inertia around the x axis of each element in portion B, the product moment of area of one band is obtained,

$$\Delta I_{t,xy}^{nl} = \sum_{l=1}^{nl} (dI_{A,t,l,xy} - dI_{B,t,l,xy}), \quad (4.17)$$

By adding all product moment of area of each band, we can have the product moment of area of the first flute.

$$I_{xy} = \sum_{t=1}^{nt} \Delta I_{t,xy}^{nl}. \quad (4.18)$$

Supposed the cutter has n tooth, thus, the area moment of inertia of each flute can be calculated by rotating an angle $\frac{2\pi}{n}$, from its previous one. Furthermore, every tooth can be

considered as a new coordinate system rotated relative to the previous one by $\frac{2\pi}{n}$. To

calculate this, the product moment of area is also required.

Considering the new coordinate system that is rotated relative to the original one by an

angle $\frac{2\pi}{n}$, then, the coordinates (P'_x, P'_y) in the new system can be calculated in terms of the

coordinates (P_x, P_y) in the original one.

$$P'_x = P_x \cdot \cos\left(\frac{2\pi}{n}\right) - P_y \cdot \sin\left(\frac{2\pi}{n}\right), \quad (4.19)$$

$$P'_y = P_x \cdot \sin\left(\frac{2\pi}{n}\right) + P_y \cdot \cos\left(\frac{2\pi}{n}\right). \quad (4.20)$$

All infinitesimal areas don't change. Substituting above now coordinates into the area moments of inertia equations, the area moments of inertia in new tooth can be obtained,

$$I'_x = \frac{I_x + I_y}{2} + \frac{I_x - I_y}{2} \cos\left(2 \cdot \frac{2\pi}{n}\right) + I_{xy} \cdot \sin\left(2 \cdot \frac{2\pi}{n}\right), \quad (4.21)$$

$$I'_y = \frac{I_x + I_y}{2} - \frac{I_x - I_y}{2} \cdot \cos\left(2 \cdot \frac{2\pi}{n}\right) - I_{xy} \cdot \sin\left(2 \cdot \frac{2\pi}{n}\right), \quad (4.22)$$

And the product moment of area can be obtained.

$$I'_{xy} = -\frac{I_x - I_y}{2} \cdot \sin\left(2 \cdot \frac{2\pi}{n}\right) + I_{xy} \cdot \cos\left(2 \cdot \frac{2\pi}{n}\right), \quad (4.23)$$

where $\frac{2\pi}{n}$ is the angle of rotation.

I_x , I_y and I_{xy} are the area moments of inertia and the product moment of area in the original coordinate system.

I'_x , I'_y and I'_{xy} are the area moments of inertia and the product moment of area in the rotated new coordinate system.

In the first tooth, the area moments of inertia and the product moment of area are

$$I_x^1 = I_x,$$

$$I_y^1 = I_y$$

$$I_{xy}^1 = I_{xy}$$

Applying to every tooth on cutter flute, from the second one to last one, the area moment of inertia and product moment of area on every tooth can be expressed,

$$I_x^m = \frac{I_x^{m-1} + I_y^{m-1}}{2} + \frac{I_x^{m-1} - I_y^{m-1}}{2} \cdot \cos\left(2 \cdot \frac{2\pi}{n}\right) + I_{xy}^{m-1} \cdot \sin\left(2 \cdot \frac{2\pi}{n}\right), \quad (4.24)$$

$$I_y^m = \frac{I_x^{m-1} + I_y^{m-1}}{2} - \frac{I_x^{m-1} - I_y^{m-1}}{2} \cdot \cos\left(2 \cdot \frac{2\pi}{n}\right) - I_{xy}^{m-1} \cdot \sin\left(2 \cdot \frac{2\pi}{n}\right), \quad (4.25)$$

$$I_{xy}^m = -\frac{I_x^{m-1} - I_y^{m-1}}{2} \cdot \sin\left(2 \cdot \frac{2\pi}{n}\right) + I_{xy}^{m-1} \cdot \cos\left(2 \cdot \frac{2\pi}{n}\right), \quad (4.26)$$

$$m \in \{2:n\}$$

Thus the area moment of inertia of the cutter can be calculated.

$$I_x = \sum_{m=1}^n I_x^m,$$

$$I_y = \sum_{m=1}^n I_y^m,$$

$$I_{xy} = \sum_{m=1}^n I_{xy}^m.$$

If a cutter size is scaled by S , all coordinates on cutter flute are scaled by S . The new coordinates (P'_x, P'_y) is,

$$P'_x = S \cdot P_x, \quad (4.27)$$

$$P'_y = S \cdot P_y. \quad (4.28)$$

The original width of the band Δr is the distance between two points, so new one becomes,

$$\Delta r' = S \cdot \Delta r. \quad (4.29)$$

The original length of the band ΔL is the distance between two points, so new one becomes,

$$\Delta L' = S \cdot \Delta L. \quad (4.30)$$

The new area moment of inertia of each element around the x axis becomes

$$dl_x' = y^2 \cdot dA = P_y'^2 \cdot \Delta r' \cdot \Delta L' = S^4 \cdot dl_x, \quad (4.31)$$

$$I_x' = S^4 \cdot I_x. \quad (4.32)$$

The new area moment of inertia of each element around the y axis becomes

$$dl_y' = x^2 \cdot dA = P_x'^2 \cdot \Delta r' \cdot \Delta L' = S^4 \cdot dl_y, \quad (4.33)$$

$$I_y' = S^4 \cdot I_y. \quad (4.34)$$

The product moment of area can be calculated.

$$dl_{xy}' = x \cdot y \cdot dA = P'_x \cdot P'_y \cdot \Delta r' \cdot \Delta L' = S^4 \cdot dl_{xy}, \quad (4.35)$$

$$I'_{xy} = S^4 \cdot I_{xy}. \quad (4.36)$$

If dividing the cutting tool into layers along the tool axis, which has a layer thickness dz , for different layer, the area moment of inertia would be different due to the lag angle of helix curve shape cutting edges. The area moment of inertia of different layer can be calculated by rotating the reference one a lag angle ψ_j , which can be obtained in Chapter 2.

$${}^jI_x = S_j^4 \cdot \left(\frac{I_x + I_y}{2} + \frac{I_x - I_y}{2} \cdot \cos(2 \cdot \psi_j) + I_{xy} \cdot \sin(2 \cdot \psi_j) \right), \quad (4.37)$$

$${}^jI_y = S_j^4 \cdot \left(\frac{I_x + I_y}{2} - \frac{I_x - I_y}{2} \cdot \cos(2 \cdot \psi_j) - I_{xy} \cdot \sin(2 \cdot \psi_j) \right), \quad (4.38)$$

$${}^jI_{xy} = S_j^4 \cdot \left(-\frac{I_x - I_y}{2} \cdot \sin(2 \cdot \psi_j) + I_{xy} \cdot \cos(2 \cdot \psi_j) \right). \quad (4.39)$$

4.5 Calculate of Area Moment of Inertia on the Gash and the Neck

Due to the fact that the cross-section on the gash or the neck of cutter is not regular, this cross-section shape can be taken by CAD software, such as CATIA. Two demonstration examples are shown in Figs 4.2.1 and 4.2.2.

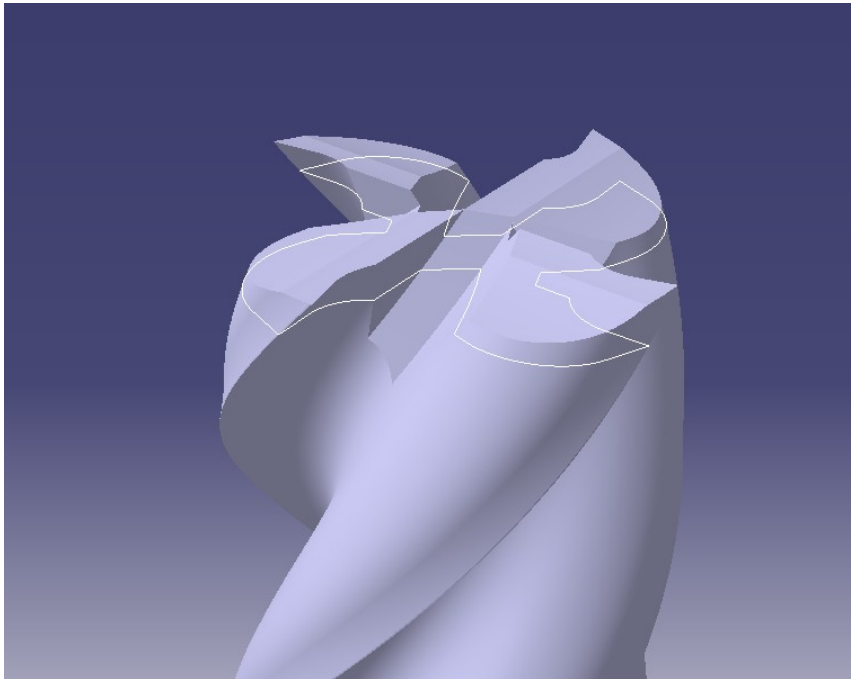


Figure 4.2.1. Illustration of irregular gash cross-section shape.

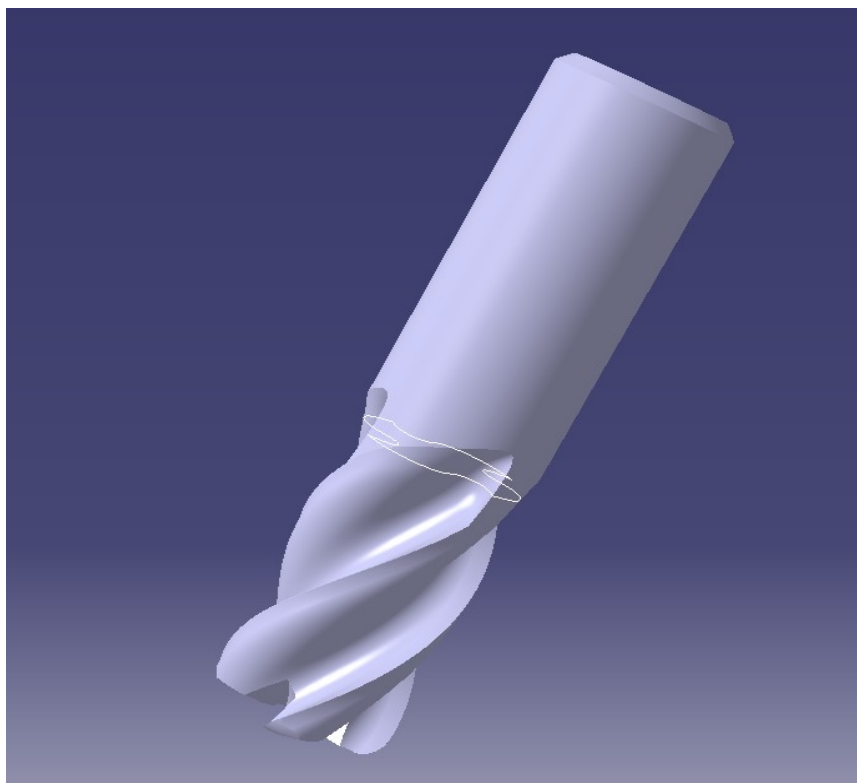


Figure 4.2.2. Illustration of irregular neck cross-section shape.

We can use general method to calculate the area moment of inertia. The differential method will be shown following.

The x-axis scalar is

$$n_t = 100 ,$$

$$t \in \{1:n_t\} .$$

The y-axis scalar is

$$n_l = 100 ,$$

$$l \in \{1:n_l\} .$$

First find out all point include this area, see Figs 4.3.1 and 4.3.2.

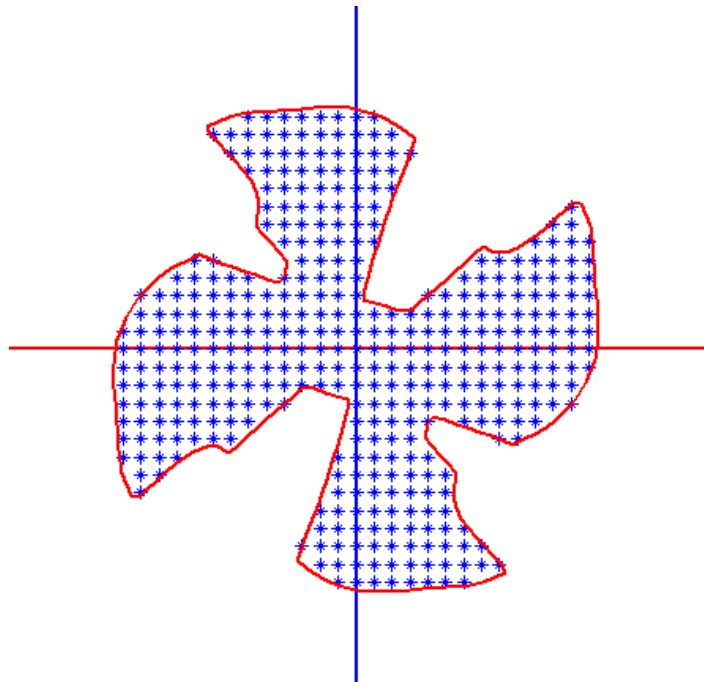


Figure 4.3.1. The differential method on the gash cross-section.

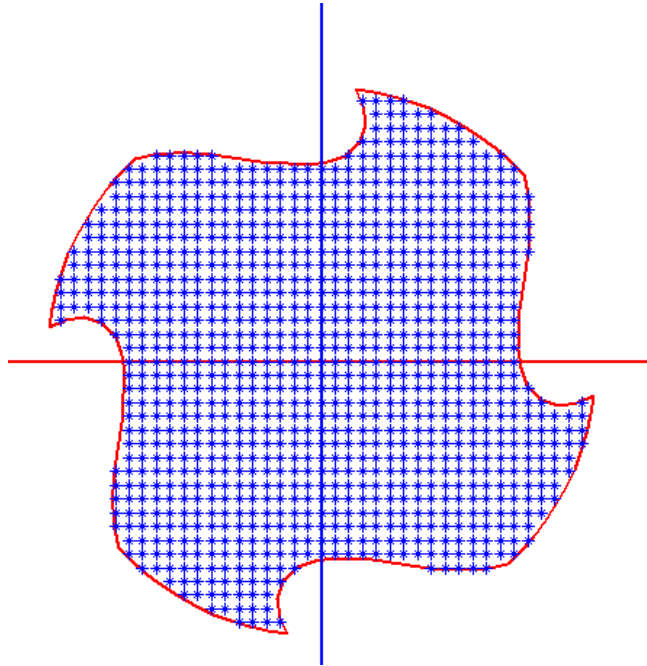


Figure 4.3.2. The differential method on the neck cross-section.

Then calculate each small area, see Figs 4.4.1. and 4.4.2.

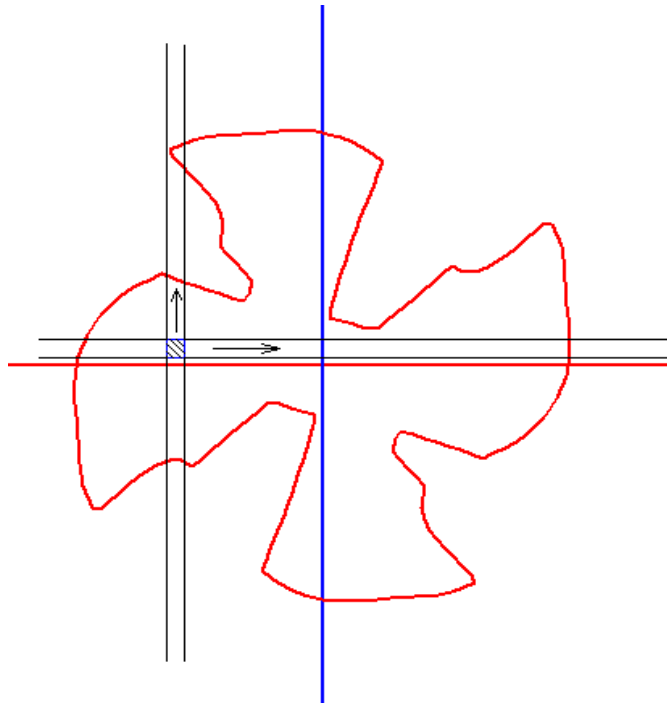


Figure 4.4.1. The searching method on the gash cross-section.

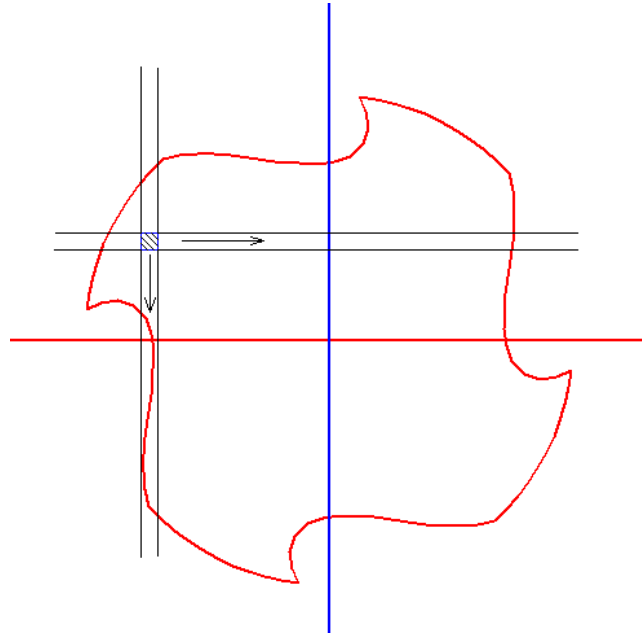


Figure 4.4.2. The searching method on the neck cross-section.

The thickness Δt and the length Δl on every infinitesimal band is

$$\Delta t = \Delta l = \frac{2 \cdot R}{n_t} . \quad (4.40)$$

For gash, the area moment of inertial can be calculated based on the below differential equations developed. Every infinitesimal area is enclosed by Δt and Δl in this area.

$$dA = dt \cdot dl = \Delta t \cdot \Delta l . \quad (4.41)$$

The area moment of inertia of each element around the x axis of each element is

$$dl_{t,l,x} = l^2 \cdot dA . \quad (4.42)$$

The area moment of inertia of each element around the y axis of each element is

$$dl_{t,l,y} = t^2 \cdot dA . \quad (4.43)$$

The product moment of area of each element is,

$$dl_{t,l,xy} = t \cdot l \cdot dA. \quad (4.44)$$

Thus the area moment of inertia of the cutter on the gash and on the neck can be calculated.

$$I_x = \sum_{i=1}^n dl_{t,l,x},$$

$$I_y = \sum_{i=1}^n dl_{t,l,y},$$

$$I_{xy} = \sum_{i=1}^n dl_{t,l,xy}.$$

4.6 Result Analysis

4.6.1 Influence of the Cutting Flutes

In Table 4.1, the calculation results of the area moment of inertia of cutting tools with different diameters on same layer are shown. In this example, for each cutting tools, $\alpha_0 = 8$, $\alpha_1 = 6$, $\alpha_2 = 10$, and $\alpha_3 = 30$, the area moments of inertia for at different positions are shown in Table 4.1. Those four parameters of cutters from column 3 to 6 are the same for the same diameter. Column 1 is the diameter and column 2 shows the number of flutes. From Figs 4.5 and 4.6, apparently, using approximate method, no matter how many flutes, the area moment of inertia is a constant, but by using this new proposed method, the area moment of inertia is changed with different flutes, the maximum deviation is about 30%. If the cross section is symmetric, product moment of inertia is equals to 0, the area moment of inertia around axis are the same. However, for a 2-blade cutter, the area moment of inertia about x axis and y axis are completely different. Actually, in many manufacturing plants, 2 blades cutters are largely applied for the roughing machining, the area moments of inertia around different axis are quite different. If using approximate method, the final result for a 2-blade cutter, no matter how hard work, the deflection is not accurate, and the compensation of the CNC tool paths is not accurate. The surface error is not accurate enough, either.

Table 4.1. Area of moment of inertia of different end-mills.

Ra. (mm)	Flute No.	r ₀ deg.	l _{AB} (mm)	l _{DE} (mm)	l _{EF} (mm)	I _x (mm ⁴)	I _y (mm ⁴)
3	2	2	0.6	1	0.4	20.76	31.82
	3					33.17	33.17
	4					36.12	36.12
	5					38.82	38.82
	6					41.06	41.06
4	2	2.8	0.8	1	0.4	72.32	105.29
	3					106.18	106.18
	4					113.55	113.55
	5					121.17	121.17
	6					127.52	127.52
5	2	3.6	1.0	2	1	231.76	290.85
	3					325.87	325.87
	4					337.60	337.60
	5					353.37	353.37
	6					364.83	634.83
6	2	4.4	1.2	2	1	441.55	601.92
	3					620.11	620.11
	4					671.70	671.70
	5					683.82	683.82
	6					730.86	730.86
7	2	5.2	1.2	2.6	1.4	856.15	1147.13
	3					1261.82	1621.82
	4					1290.12	1290.12
	5					1351.80	1351.80
	6					1438.24	1438.24
8	2	6.0	1.4	2.6	1.4	1358.73	1903.22
	3					2028.31	2028.31
	4					2136.79	2136.79
	5					2261.82	2261.82
	6					2347.82	2347.82

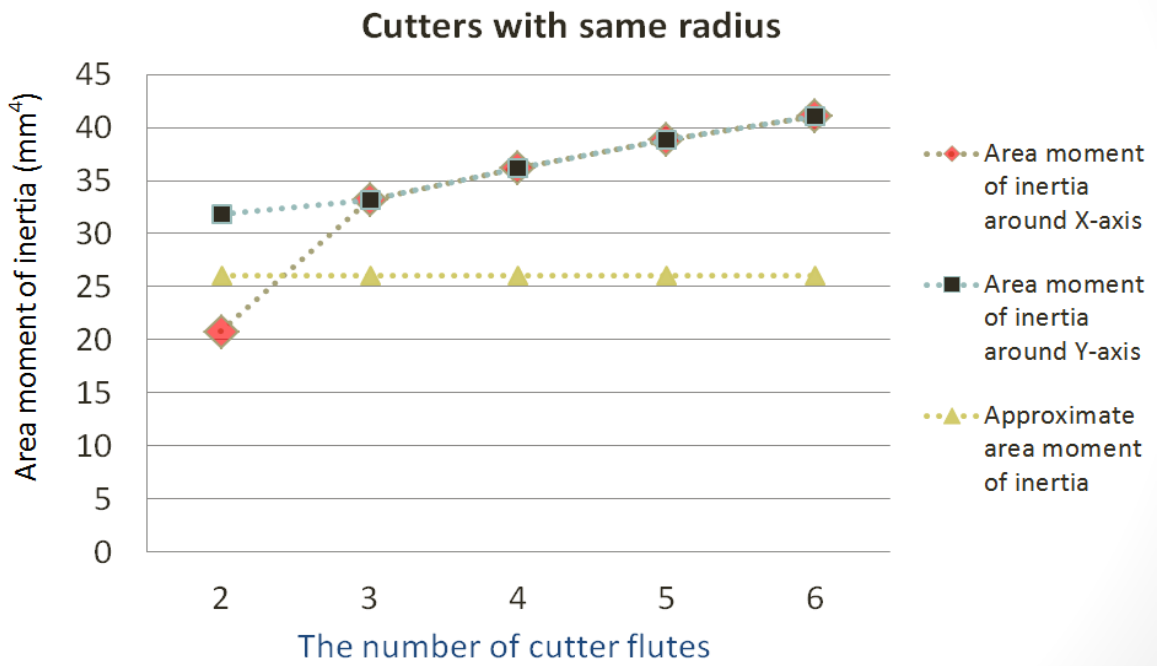


Figure 4.5. Area moment of inertia and number of flutes.

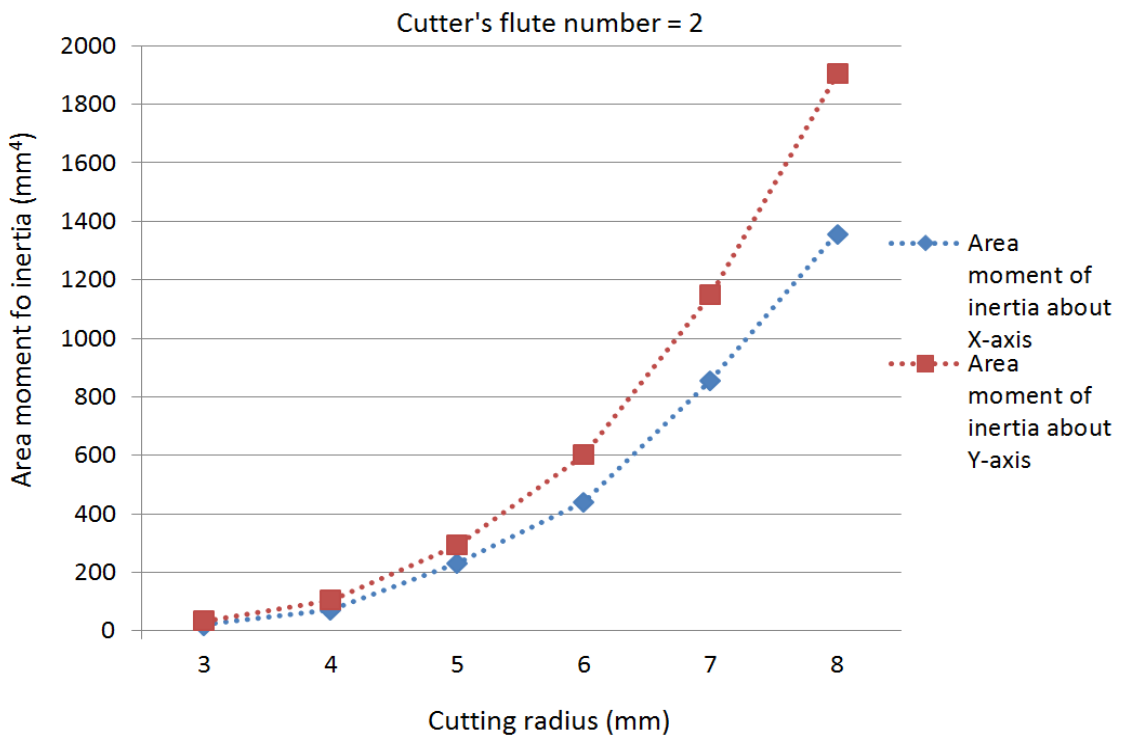


Figure 4.6. Area moment of inertia of cutter.

4.6.2 Influence of the Cutting Radius

For a symmetric section of a fillet tapered end-mill, at any position of the cutting edges along the tool axis, the area moment of inertia around the x and y axes are the same at the same layer. For example, for a fillet tapered cutting tool, $R = 3$, $R_s = 5$, taper angle = 3, $r_0 = 1.8$, $I_{EF} = 0.6$, $I_{ED} = 1.0$, $I_{AB} = 0.8$, $\alpha_1 = 8^\circ$, $\alpha_2 = 12^\circ$, and $\alpha_3 = 30^\circ$, the cutting edge, flutes shape information and the area moments of inertia for at different positions are shown in Table 4.2. In Figure 4.7, the data from Table 4.2 is better demonstrated.

Table 4.2. Data for symmetric section fillet tapered end mills.

Parameters of cutter											
Cutting edge (mm)					Flute (mm)						
R	Rs	L	a	θ	r0	$\alpha 1$	$\alpha 2$	$\alpha 3$	I_{AB}	L_{EF}	L_{DE}
3	5	40	3°	30°	1.8	8°	12°	30°	0.8	0.6	1.0
Symmetric section (n=4)						Area moment of inertia					
z	Helix Lag Angle		r	S	Ix		Iy				
-3.0000	0.0000		5.0000	1.0000	37.859		37.859				
-0.9971	0.3124		7.8294	1.5659	227.628		227.628				
1.0027	0.4584		8.0567	1.6113	255.197		255.197				
3.0025	0.6010		8.1615	1.6323	268.763		268.763				
5.0024	0.7418		8.2663	1.6533	282.863		282.863				
7.0023	0.8808		8.3711	1.6742	297.439		297.439				
9.0021	1.0180		8.4759	1.6952	312.646		312.646				
11.0019	1.1536		8.5807	1.7161	328.352		328.352				
13.0018	1.2875		8.6855	1.7371	344.722		344.722				
15.0016	1.4199		8.7903	1.7581	361.696		361.696				
17.0015	1.5506		8.8951	1.7790	379.204		379.204				
19.0013	1.6798		8.9999	1.8000	397.429		397.429				
21.0012	1.8076		9.1047	1.8209	416.211		416.211				
23.0010	1.9338		9.2096	1.8419	435.746		435.746				
25.0009	2.0587		9.3144	1.8629	455.961		455.961				
27.0008	2.1821		9.4192	1.8838	476.769		476.769				
29.0006	2.3042		9.5240	1.9048	498.387		498.387				
31.0005	2.4249		9.6288	1.9258	520.732		520.732				
33.0003	2.5443		9.7336	1.9467	543.707		543.707				
35.0001	2.6625		9.8384	1.9677	567.551		567.551				
37.0000	2.7794		9.9432	1.9886	592.051		592.051				

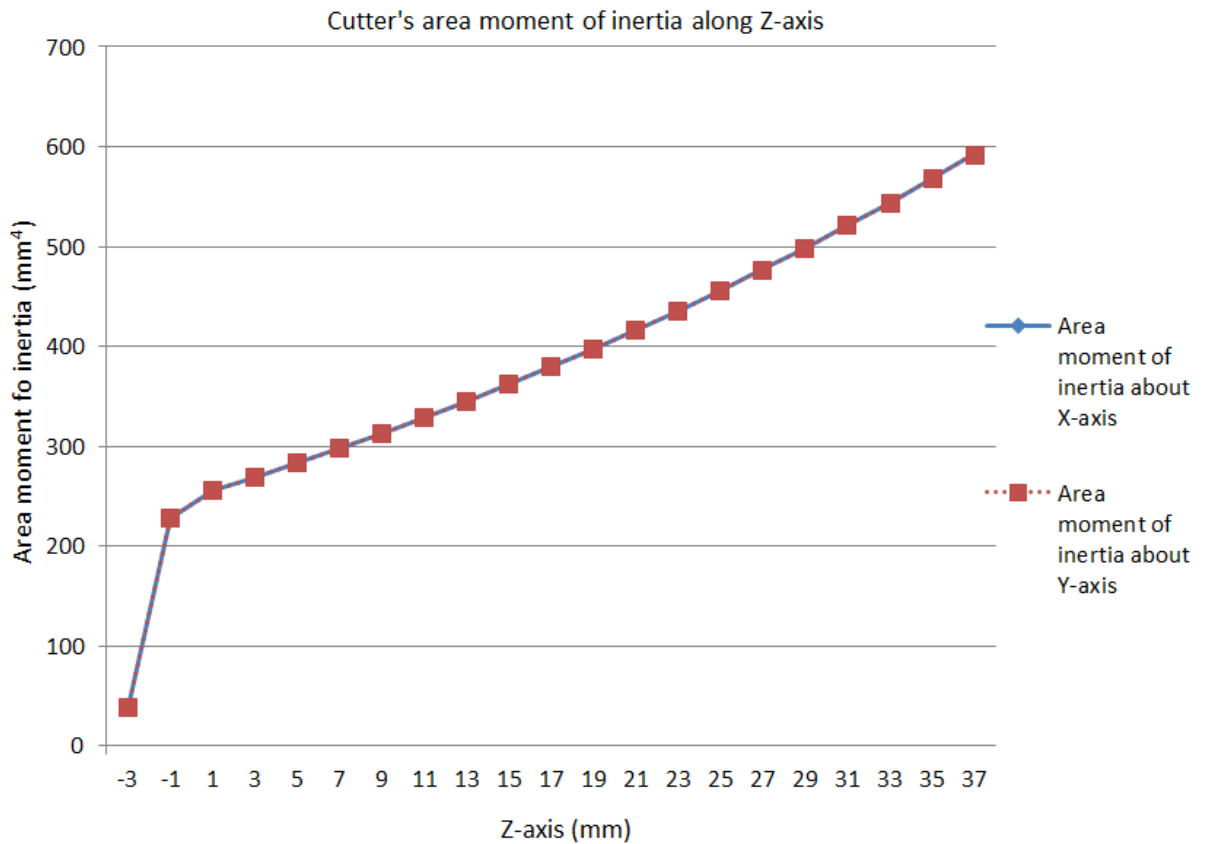


Figure 4.7. Area moment of inertia along axis-z.

For a symmetric section of a cutting tool, the area moments of inertia around the x axis equates to the area moments of inertia around the y axis, but obviously, for an asymmetric section of a cutting tool, the area moment of inertia around the x axis and y axis are not equal to each other.

In this work, the product area moments of inertia for any kind of fillet tapered end mills equates to zero, no matter how many cutting flutes, and no matter how shapes of cross-section of cutter.

4.6.3 The Results on the Gash and the Neck

In this section, the method for calculating area moment of inertia on the gash and the neck is elaborated. To demonstrate this method better, this method is applied to a solid carbide flat end-mill. The parameter values of the tool are listed in Table 4.3. Thirty experiments are also conducted and the corresponding results are provided in Table 4.3. It is evident that it is more accurate calculation for the area moment of inertia. The results of the accurate area moment of inertia are plotted in Figure 4.8.

Table 4.3. The area moment of inertia on the gash and on the neck.

Flute		Parameters of cutting flute			Area moment of inertia (mm ⁴)								
Ra. (mm)	Flute No.	α_1 Deg.	α_2 Deg.	α_3 Deg.	Gash			Flank			Neck		
					Z (mm)	I_x	I_y	Z (mm)	I_x	I_y	Z (mm)	I_x	I_y
10	4	12	2	12	1	1995	1837	6	3120	3120	31	3190	3190
					1.5	2791	2578	10	3120	3120	32	3438	3438
					2	2944	2734	12	3120	3120	33	3794	3794
					2.5	3028	2834	15	3120	3120	34	4258	4258
					3	3081	2924	17	3120	3120	35	4868	4868
					3.5	3057	2938	20	3120	3120	36	5606	5606
					4	3112	3040	22	3120	3120	37	6452	6452
					4.5	3091	3050	23	3120	3120	38	7232	7232
					5	3134	3129	25	3120	3120	39	7800	7800
					5.5	3116	3116	30	3120	3120	40	7854	7854

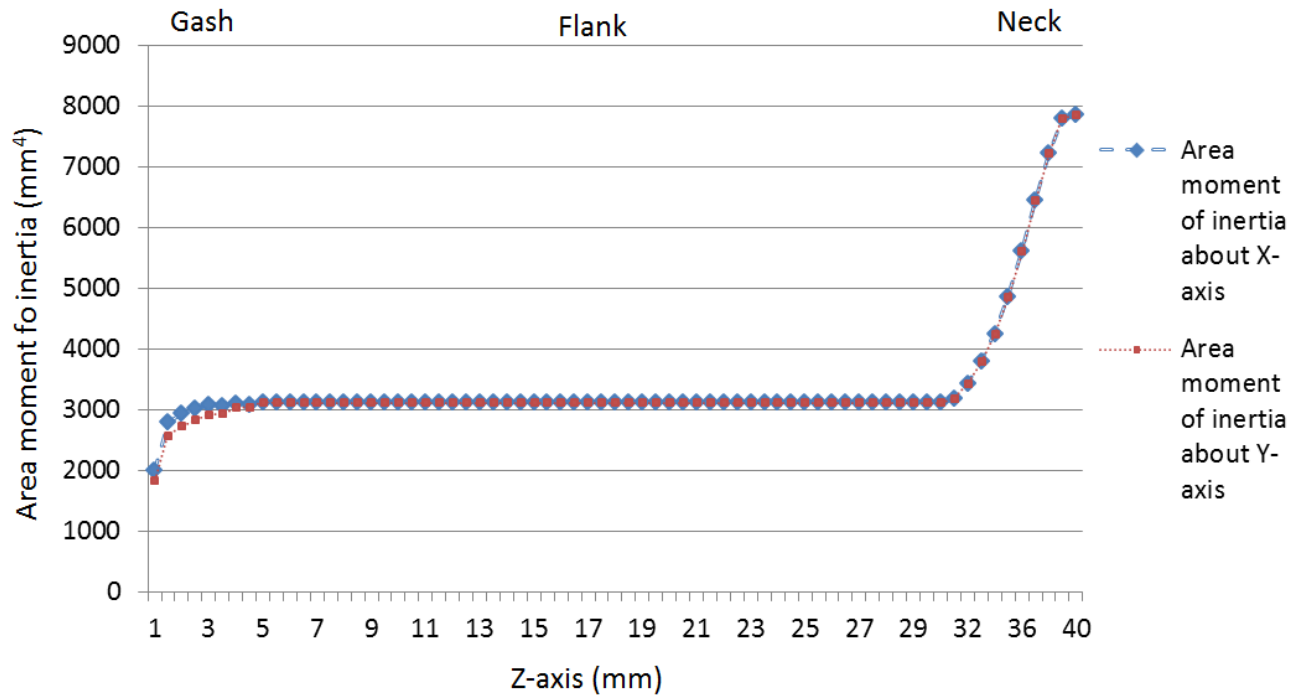


Figure 4.8. Area moment of inertia on the gash and neck cross-section.

4.6.4 Comparison between Two Different Methods

In this research, two methods for calculating area moment of inertia on different cutter positions are proposed. The calculation efficiency and accuracy of these two methods is shown in Table 4.4. A circle with 10mm radius is used as reference to compare these two methods' accuracy. Results show that the special method is more efficient and accurate.

Table 4.4. The calculation efficiency.

Cutter positions	1 st scalar	2 nd scalar	Calculation steps	Area moment of inertia of circle	Area moment of inertia of methods
Special method on Cutting edge	10^3	10^2	10^5	7854mm ⁴	7854mm ⁴
General method on Gash or neck	10^3	10^2	$n \times 10^5$		7800mm ⁴

where n is the number of intersections points from CAD software.

5.1 Introduction

The cutting edges and the cutting flutes of an end-mill significantly affect cutter's area moment of inertia; furthermore, they are also the most important factors to affect cutting force. In order to find the relationship between different cutter geometry and area moment of inertia, the area moments of inertia of several cutting tools with the different flutes will be calculated and the results will be compared. In the examples, the design parameters such as the rake, relief, clearance angles, and the number of flutes of the cutting tool are the variable. In order to apply the proposed CAD model for simulation, the cutting simulation software, ThirdWave System, will be used to predict the cutting force. Third Wave Systems' analysis software is the ideal tool for designers in the metalworking industry. With the software suite, the time and the money can be reduced during designing, testing, and delivering to market for new cutting tools. Finally in this research, two simulations will be conducted, in each simulation, different cutters model with different parameters can be applied for predicting the cutting force.

5.2 Influence of the Rake Angle to Area Moment of Inertia

In this section, some parameters will be considered as to how they affect the area moment of inertia. For example, rake angle α_1 is taken into consideration. In Table 5.1, based on the above CAD cutters' models, the result of comparison is shown. As the change of the rake angle, the area moment of inertia of the cutting tool changes too. In Figs 5.1, the data from Table 5.1 is better demonstrated.

Table 5.1. Comparison of the effect of the rake angle.

Flute		Parameters of cutting flute								Area moment of inertia	
R. (mm)	Flute no.	r_0 (mm)	l_{AB} (mm)	l_{DE} (mm)	l_{EF} (mm)	α_1 deg.	α_2 deg.	α_3 deg.	α_0 deg.	I_x (mm ⁴)	I_y (mm ⁴)
10	4	7	1.6	2.4	1.2	2	12	30	8	3977.21	3977.21
						5				4020.71	4020.71
						8				4054.56	4054.56
						11				4096.77	4096.77
						14				4128.18	4128.18
						17				4165.20	4165.20

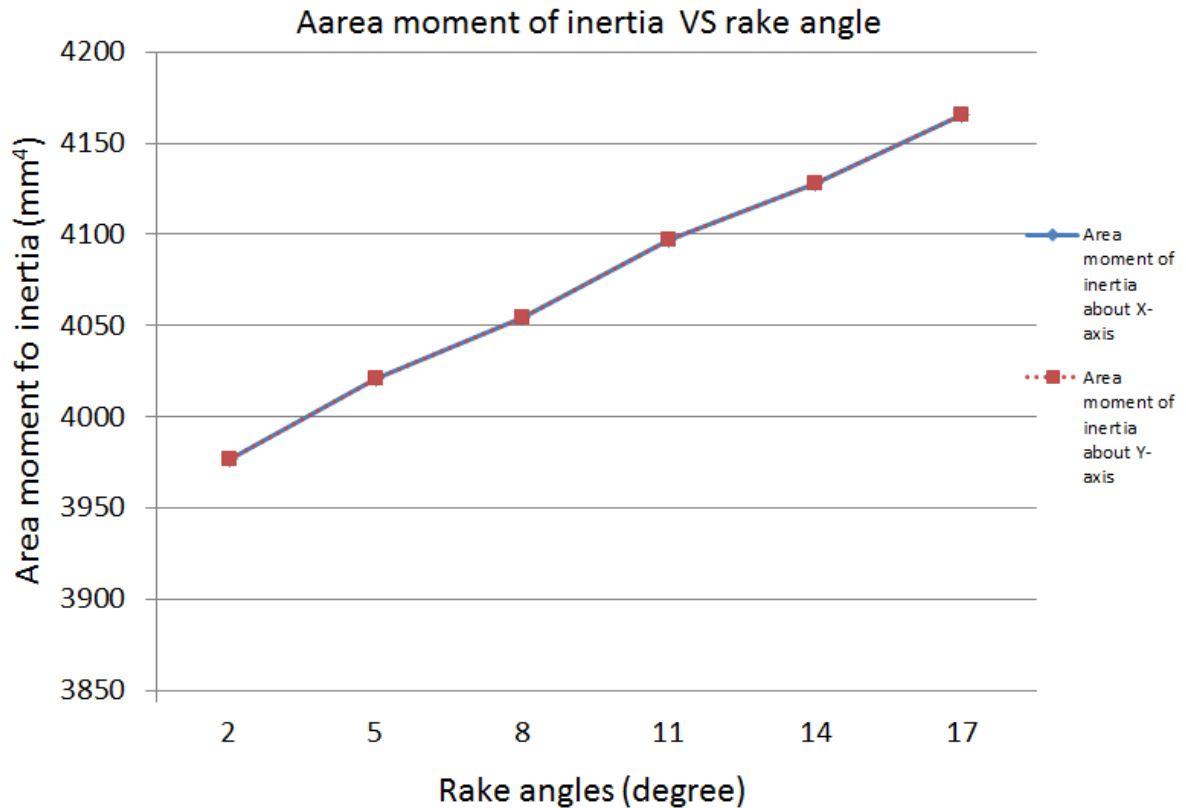


Figure 5.1. The Effect of α_1 for four cutting teeth.

5.3 Cutting Force Analysis based on the Change of Rake Angle

About the prediction of cutting force, Third Wave Systems can be applied. Third Wave Systems is the simulation software for high speed machining processes. It can provide many cutting parameters under some cutting conditions, such as cutting force, cutting temperature and stress and so on. In Table 5.2, the geometry parameters of tools and work piece based on CAD model in this research are listed. Table 5.3 the simulation parameters of Third Wave Systems are listed. It is clear that, as the change of the rake angle, the maximum cutting force changes too.

Table 5.2. The parameters of cutter and the geometry of workpiece.

Tool geometry parameters		Workpiece parameters	
Cutting radius	10mm	Workpiece width	1mm
Core radius	7mm		
Cutting edges	4	Workpiece height	0.5mm
Rake angle	5°/11°/17°		
Relief angle	12°		
Clearance angle	30°	Workpiece length	1mm
Length of cutter	4mm/20mm		
Helix	30°		

Table 5.3. The parameters of simulation.

Machining parameters		FEA parameters	
Tool material	Carbide-Grade-P	Min. element edge length (chip bulk)	0.010305mm
Workpiece material	Ti-6Al-4V	Min. element edge length (cutter edge)	0.00788mm
Spindle speed (RPM)	1273		
Feed per tooth (mm/tooth)	0.03	Radius of refined region (cutter edge)	0.03897mm
Radial width of cut (mm)	2		
Angle of rotation	10°	Maximum element size	0.5mm
Milling option	Side milling	Minimum element size	0.008mm

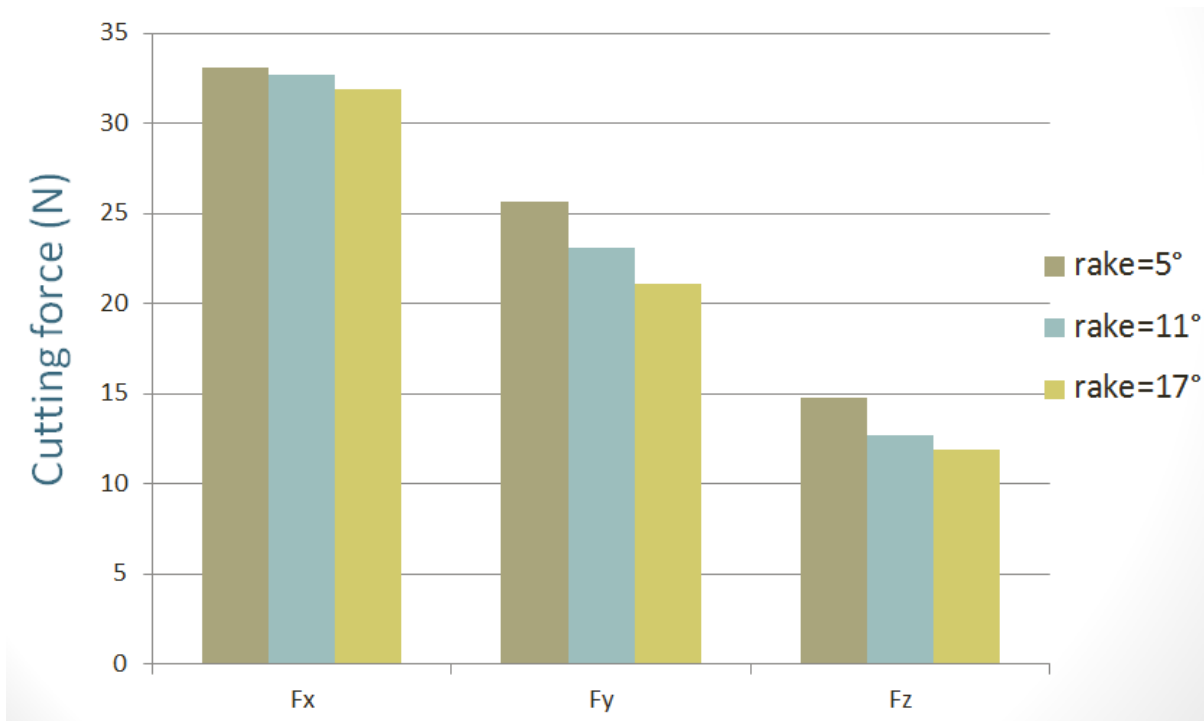


Figure 5.3. The plot of the maximum cutting force curve at different rake angles.

In Figure 5.3, the result from ThirdWave System is better demonstrated. However, in CNC machining, if cutter's rake angle is too big, cutter's rigidity will come down. Generally, rake angle of milling cutters is smaller than 20 degree. So considering this situation, based on the simulation results, the cutter with 17 degree rake angle is better.

5.4 Cutting Force Analysis based on the Change of Helical Angles

Another cutting simulation is to analysis cutting force based on different helical angles of cutting edge. In Table 5.4, the geometry parameters of tools and work piece based on CAD model in this research are listed. The simulation parameters of Third Wave Systems are same with last simulation.

Table 5.4. The parameters of cutter and the geometry of workpiece.

Tool geometry parameters		Workpiece parameters	
Cutting radius	10mm	Workpiece width	1mm
Core radius	7mm		
Cutting edges	4	Workpiece height	0.5mm
Rake angle	11°		
Relief angle	12°		
Clearance angle	35°/40°/45°	Workpiece length	1mm
Length of cutter	4mm/20mm		
Helix	30°		



Figure 5.4. The plot of the maximum cutting force curve at different helical angles.

In Figure 5.4, the result from ThirdWave System is better demonstrated. It is clear that, as the change of the helical angles, the maximum cutting force changes too. During CNC machining, if the helical angle is too big, it is difficult to move out chips. So considering

these situations, based on the simulation results, for different cutting style and different workpiece material, we can find what geometry is better for cutting tools. According to this simulation, the cutter with 40 degree helical angle is better.

6.1 Conclusions

In this work, a parametric modeling of the carbide end mills has been constructed which can be automatically and efficiently built 3-D solid model for CAD model, and an accurate approach to compute the area moments of inertia of the toroidal tapered end mills has also been derived. More specifically, the research work includes: (1) establishment of a free-form mathematical model of a helix curve cutting edge, (2) establishment of a free-form mathematical model of a cutting flute, and (3) calculation of the area moment of inertia of the cutting tool. The purpose of building the free-form mathematical model of the cutting tool is that, in all the current CAD/CAM software, all solid models are represented by the free-form curves and the surfaces. This makes: (1) the prediction of machined error and deflection more accurate, (2) when simulating the machined surface in CAM software, the displayed machined surface is accurate enough, and (3) it is easier to control the geometry of CAD model.

The data tables and figures are shown to clarify the difference of the area moment of inertia of the real design models of the cutting tool. And, some other parameters of the cutting flutes are also listed. This work can be used, together with an existing cutting force calculation method, to accurately predict cutter deflections during milling in order to

compensate them in CNC tool paths. It can also provide more precise 3-D solid models of end-mills for machining simulation by using finite element analysis.

6.2 Future Research

The following topics are suggested for a future work to expand the present research work:

- Using the built mathematic model to predict cutting force

In my current thesis, the mathematical model of cutting tool is built, which can be used in the visual machining and cutting force prediction.

- Using the built mathematic model to predict analyze of the stress of cutting tool
- The CAD model can be applied into CAE software
- The area moment of inertia can be applied into CAE software

In current trend software, the area moment of inertia is calculated by approximating the cutting tool as a cantilever. It is hoped this numerical method can be applied in the commercial software to predict the machined error and deflection.

Chapter 7 References

- (1) Engin, S., and Altintas, Y., 2001, "Mechanics and dynamics of general milling cutters. Part I: helical end mills," *International Journal of Machine Tool & manufacture*, Vol. 41, pp. 2195-2212.
- (2) Chen, W.F., Lai H.Y., and Chen, C.K., 2001, "A precision tool model for concave cone-end milling cutters," *International Journal of Advanced Manufacturing Technology*, Vol. 18, pp. 567-578.
- (3) Chen, C.B., Wang, F.S., Chang, P.C., Hwang, J.H., and Chen, W.F., 2006, "A precision design and NC manufacturing model for concave-arc ball-end cutters," *International Journal of Advanced Manufacturing Technology*, Vol. 31, pp. 283-296.
- (4) Wang, Y.T., Bao, Q.S., and Tang, Y.Y., 2002, "A manufacturing model of s-shaped ball-nosed milling cutter and error analysis in realization in industry," *International Journal of Advanced Manufacturing Technology*, Vol. 20, pp. 92-98.
- (5) Chen, C.K., and Lin, R.Y., 2001, "A study of manufacturing models for ball-end type rotating cutters with constant pitch helical flutes," *International Journal of Advanced Manufacturing Technology*, Vol. 18, pp. 157-167.
- (6) Lin, S.W., and Lai, H.Y., 2001, "A mathematical model for manufacturing ball-end cutters using a two-axis NC machine," *International Journal of Advanced Manufacturing Technology*, Vol. 17, pp. 881-888.

- (7) Tsai, Y.C., and Hsieh, J.M., 2001, "A study of a design and NC manufacturing model of ball-end cutters," *Journal of Materials Processing Technology*, Vol. 117, pp. 183-192.
- (8) Chen, W.F., and Chen, W.Y., 2002, "Design and NC machining of a toroid-shaped revolving cutter with a concave-arc generator," *Journal of Materials Processing Technology*, Vol. 121, pp. 217-225.
- (9) Chen, W.F., 2004, "A mathematical solution to the design and manufacturing problems of ball-end cutters having a cutting edge with constant angle to the axis," *Proceedings of Institute of Mechanical Engineers, Part C: Journal of Mechanical Engineering Science*, Vol. 218, pp. 301-308.
- (10) Liu, J.Y., and Chang, S.L., 2003, "Design of hob cutters for generating helical cutting tools with multi-cutting angles," *International Journal of Machine Tools & Manufacture*, Vol. 43, pp. 1185-1195.
- (11) Sheth, D.S., and Malkin, S., 1973, "CAD/CAM for geometry and process analysis of helical flute machining," *Annals of CIRP*, Vol. 22, No. 1, pp. 157-164.
- (12) Kaldor, S., Rafael, A.M., and Messinger, D., 1990, "On the CAD of profiles for cutters and helical flutes – geometrical aspects," *Annals of CIRP*, Vol. 39, No. 1, pp. 129-132.
- (13) Kang, S.K., Ehmann, K.F., and Lin, C., 1996, "A CAD approach to helical flute machining, I. mathematical model and model solution," *International Journal of Machine Tools & Manufacturing*, Vol. 36, No. 1, pp. 141-153.
- (14) Xu, X.J., Bradley, C., Zhang, Y.F., Loh, H.T., and Wong, Y.S., 2002, "Tool-path generation for five-axis machining of free-form surfaces based on accessibility analysis," *international Journal of Production Research*, Vol. 40, No. 14, pp. 3253-3274.

- (15) Yin, Z., 2004, "Rough and finish tool-path generation for NC machining of freeform surfaces based on a multiresolution method," *Computer-Aided Design*, Vol. 36, pp. 1231–1239.
- (16) Razavi, S.E., and Milner, D.A., 1983, "Design and manufacture of free-form stances by cross-sectional approach," *Journal of Manufacturing Systems*, Vol. 2, No. 1, pp.69-77.
- (17) Piegl, L. and Tiller, W., The NURBS Book, 2nd Edition, *Springer*.